Journal of Solution Chemistry (2019) 48:702–731
https://doi.org/10.1007/s10953-019-00882-2

A Search for the Protonation Model with Thermodynamic Dissociation Constants and (Extra)-Thermodynamics of Nilotinib Hydrochloride (TASIGNA)

Milan Meloun[1] · **Lucie Pilařová**[1] · **Milan Javůrek**[2] · **Tomáš Pekárek**[3]

Received: 8 October 2018 / Accepted: 16 February 2019 / Published online: 20 May 2019

Abstract
Nilotinib hydrochloride (AMN107, TASIGNA, Novartis) is used to treat adults with chronic myeloid leukemia (CML), a type of leukemia. It is a novel, orally active BCR-ABL tyrosine kinase inhibitor derived from aminopyrimidine that is 30 times more effective against CML cells than is Imatinib. The nonlinear regression of the *A* versus pH spectra with REACTLAB and SQUAD84 and of the pH-titration curve with ESAB determined the four close and consecutive dissociation constants in the 11 steps of the newly proposed procedure. Prediction of pK_a performed by MARVIN, PALLAS and ACD/Percepta determined the protonation sites. The sparingly soluble nilotinib hydrochloride denoted as L forms four water-soluble LH^+, LH_2^{2+}, LH_3^{3+}, and LH_4^{4+} cations. Although the adjusted pH has less effect on the absorbance changes in the chromophore, four thermodynamic dissociation constants were reliably determined: $pK_{a1}^T = 3.60 \pm 0.04$, $pK_{a2}^T = 4.42 \pm 0.07$, $pK_{a3}^T = 4.71 \pm 0.04$, and $pK_{a4}^T = 4.84 \pm 0.03$ at 25 °C and $pK_{a1}^T = 3.61 \pm 0.11$, $pK_{a2}^T = 4.29 \pm 0.18$, $pK_{a3}^T = 4.49 \pm 0.02$, and $pK_{a4}^T = 5.05 \pm 0.03$ at 37 °C, and by regression analysis of potentiometric titration curves with ESAB, $pK_{a1}^T = 3.74 \pm 0.01$, $pK_{a2}^T = 4.05 \pm 0.01$, $pK_{a3}^T = 4.25 \pm 0.01$, and $pK_{a4}^T = 4.91 \pm 0.20$ at 25 °C and $pK_{a1}^T = 3.63 \pm 0.03$, $pK_{a2}^T = 3.96 \pm 0.03$, $pK_{a3}^T = 4.18 \pm 0.03$,

Electronic supplementary material The online version of this article (https://doi.org/10.1007/s10953-019-00882-2) contains supplementary material, which is available to authorized users.

✉ Milan Meloun
milan.meloun@upce.cz
http://meloun.upce.cz

Lucie Pilařová
lucie.pilarova91@centrum.cz
http://www.upce.cz

Milan Javůrek
Milan.Javurek@upce.cz
http://www.upce.cz

Tomáš Pekárek
Tomas.Pekarek@zentiva.com

[1] Department of Analytical Chemistry, University of Pardubice, 532 10 Pardubice, Czech Republic

[2] Department of Process Control, University of Pardubice, 532 10 Pardubice, Czech Republic

[3] Development, Zentiva k.s, U kabelovny 130, 102 37 Prague, Czech Republic

and $pK_{41}^{T} = 4.81 \pm 0.05$ at 37 °C. Positive enthalpy values $\Delta H°$ at 25 °C showed that the dissociation process is endothermic and is accompanied by heat absorption. Inasmuch as the entropy values of the dissociation process $\Delta S°$ at 25 °C and 37 °C were negative, the dissociation process is reversible.

Graphical Abstract

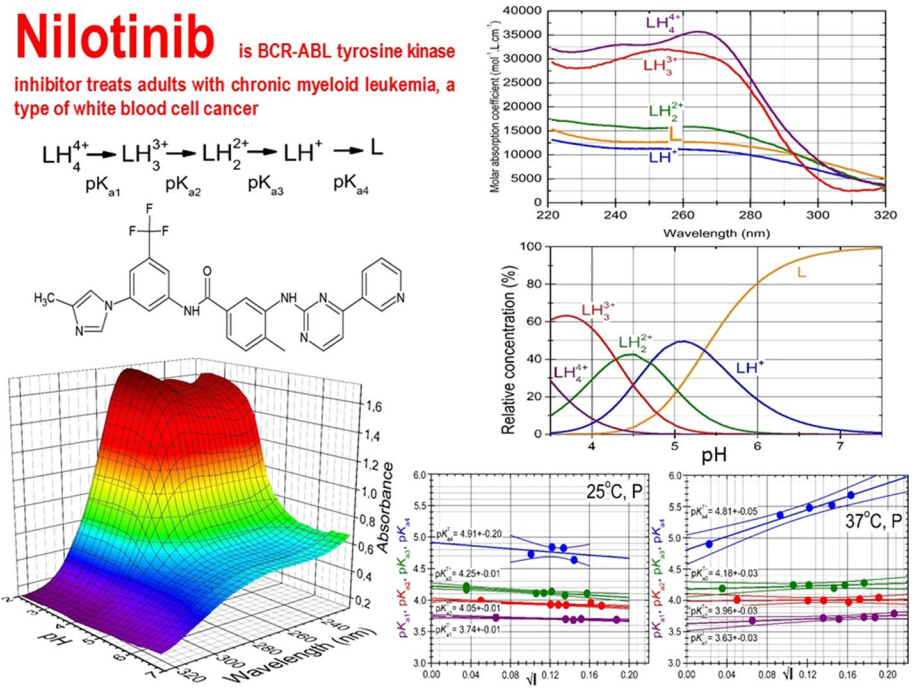

Keywords Dissociation constants · Nilotinib · Spectrophotometric titration · pH-titration · REACTLAB · SQUAD84 · ESAB

1 Introduction

Chronic myelogenous leukemia (CML) is a clonal myeloproliferative disorder characterized by the expansion of the Philadelphia chromosome Ph in hematopoietic cells resulting from reciprocal translocation of the long arms of chromosomes 9 and 22. A new fusion gene, BCR-ABL, encodes a constitutively active protein tyrosine kinase [1–3]. The development of thyrosine kinetase inhibitors for CML treatment is based on the discovery that CML stem and progenitor cells overexpress the abnormal BCR-ABL fusion protein kinase. The TKI prototype, Imatinib, selectively inhibits BCR-ABL as well as several other kinases, including the stem cell factor receptor KIT, discoidin domain receptor DDR, the platelet-derived growth factor receptor PDGFR and receptor-1-1R. Although treatment with CML has dramatically improved with Imatinib, not all patients benefit from treatment due to resistance or intolerance. As a result, research has focused on the development of stronger TKIs with the ability to bypass Imatinib resistance [1].

Nilotinib hydrochloride is a medicine used to treat adults with chronic myeloid leukemia CML, a type of leukemia. Nilotinib hydrochloride (Tasigna, AMN107, Novartis) is a novel, orally active BCR-ABL tyrosine kinase inhibitor derived from aminopyrimidine that is 30 times more effective against CML cells than is Imatinib. Imatinib acts as a competitive inhibitor of BCR-ABL at the ATP-binding site of Nilotinib hydrochloride, resulting in the inhibition of the tyrosine phosphorylation of proteins involved in intracellular signal transduction mediated by BCR-ABL. Nilotinib hydrochloride has a higher binding affinity and selectivity than Imatinib for ABL kinase. It also has 20- to 50-fold higher inhibitory activity than Imatinib in Imatinib-sensitive CML cell lines and three- to sevenfold higher activity in Imatinib-resistant cell lines. Nilotinib hydrochloride is also active in 32 of 33 Imatinib-resistant cell lines with mutant ABL kinases [4]. In summary, Nilotinib hydrochloride is highly effective and safe in patients with chronic myeloid leukemia in the chronic phase after Imatinib failure or intolerance [1].

The IUPAC chemical designation of Nilotinib hydrochloride is 4-methyl-*N*-(3-(4-methyl-1H-imidazol-1-yl)-5-(trifluoromethyl)phenyl)-3-((4-(pyridin-3-yl)pyrimidin-2-yl)amino)benzamide hydrochloride [4] with the molecular formula $C_{28}H_{23}ClF_3N_7O$ and there are various chemical names for Nilotinib hydrochloride such as UNII-K37N7BYX3X, and PubChem C28H22F3N7O·ClH, SCHEMBL434496, Tasigna (Novartis), CHEMBL255863, and DTXSID60238968. The registration number is CAS 923288-95-3. The molecular weight is 565.985 $g{\cdot}mol^{-1}$ and water solubility is 0.024 $mg{\cdot}L^{-1}$ at 25 °C (Fig. 1).

One of the most important physico-chemical characteristics of every drug is its pK_a value, which is a key physicochemical parameter influencing many biopharmaceutical characteristics in pharmacokinetic and bioavailability studies, as they reveal the deprotonation state of a molecule in a particular solvent. The dissociation constants of a compound

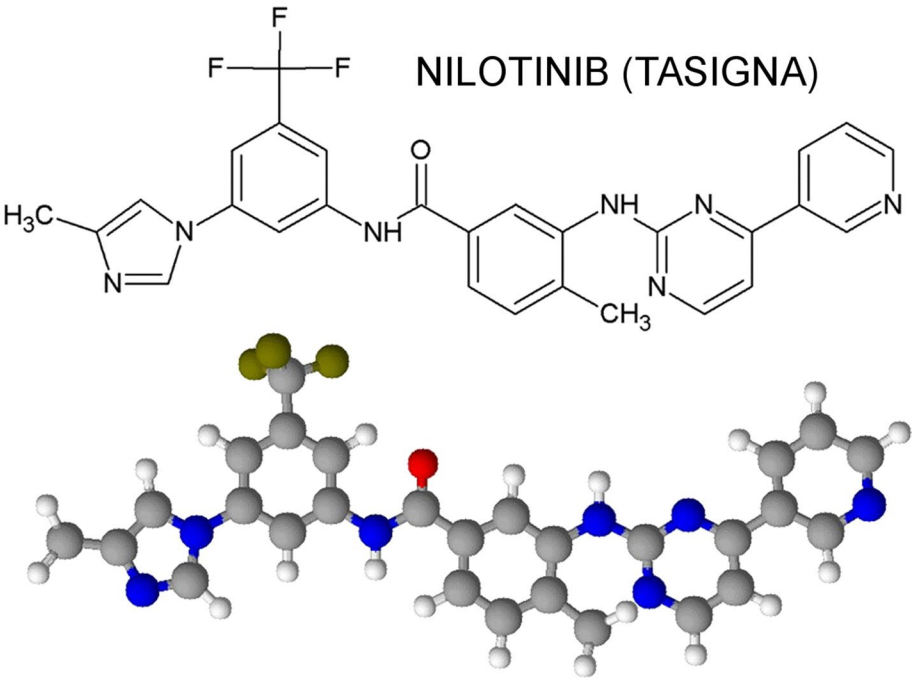

Fig. 1 Structural formula of Nilotinib

influences its lipophilicity, solubility, and permeability and play a crucial role in the characterization of its absorption, distribution, metabolism and excretion (ADME) profile [3–7]. They are very important both in the analysis of drugs and in the interpretation of their mechanisms of action. The present study is a continuation of our investigation into the dissociation equilibria of various drugs in aqueous solutions at 25 °C and 37 °C, a survey is given in Ref. [8]. The pK_a values can be either experimentally measured or theoretically predicted:

1. The dissociation constant pK_{ai} of the acid LH_i is determined by a regression analysis of potentiometric titration data also called the *pH-metric analysis* when *common parameters* (pK_{ai}, $i=1,\ldots,j$) and *group parameters* (E°, L_0, H_T) are refined. The ill-conditioned group parameters should be refined together with the common parameters (pK_{ai}), otherwise the estimates of pK_{ai} are not sufficiently accurate. The first attempt to use the least-squares methods for refining both protonation/dissociation constants (*common parameters*) and analytical concentrations (*group parameters*) was made by Sillén et al. [9–12]. More recently non-linear regression programs for analyzing potentiometric data for both common and group parameters have been applied such as ESAB [13, 14], SUPERQUAD and HYPERQUAD [15–18]. *Common parameters* are the same for all the experiments, such as dissociation constants. *Group parameters*, sometimes termed *dangerous parameters*, are those that vary from one experiment to another, such as E°, analytical concentrations, or calibration of the electrode used. For systems where the model is unknown and only guessed, this difficulty should be kept in mind and group parameters refined after the correct model has been obtained by graphical or numerical methods.
2. Spectrophotometric *UV-metric spectra analysis* [19], in particular, is a highly sensitive and convenient method to determine pK_a values in very dilute aqueous solutions since it requires only relatively simple equipment and can work with a sub-micromolar compound concentration (about 10^{-5} to 10^{-6} mol·L^{-1}), *cf. refs.* [20–22].
3. The accuracy of theoretical pK_a predictions from a molecular structure with the use of three predictive programs ACD/Percepta [23–29], MARVIN [23, 25, 26, 28, 30–33] and PALLAS was found to be the best of all nine similar programs [34].

The aim of our study was to examine the regression analysis of the pH-absorbance matrix with very small absorbance changes in the spectra of Nilotinib hydrochloride, and to carry out a pH-metric potentiometric determination of the protonation model to find suitable conditions for a reliable regression determination of all close values of the consecutive dissociation constants and to calculate the thermodynamic parameters such as enthalpy, entropy and Gibbs energy.

2 Experimental Section

2.1 Chemicals and Solutions

Nilotinib hydrochloride donated by ZENTIVA k.s. (Prague) with declared purity checked by a HPLC method and alkalimetrically was always > 99%. This drug was weighted straight into a reaction vessel resulting in a concentration of about 1.0×10^{-4} mol·L^{-1}. *Hydrochloric acid,* 1 mol·L^{-1}, was prepared by diluting a concentrated HCl (p.a., Lachema

Brno) with redistilled water and standardization against HgO and KI with a reproducibility better than 0.002 according to the equations $HgO + 4\ KI + H_2O \rightleftharpoons 2\ KOH + K_2[HgI_4]$ and $KOH + HCl \rightleftharpoons KCl + H_2O$. *Potassium hydroxide,* 1 $mol{\cdot}L^{-1}$, was prepared from the exact weight of p.a. pellets, Aldrich Chemical Company with carbon-dioxide-free redistilled water kept for 50 min prior to that in an ultrasonic bath. The solution was stored for several days in a polyethylene bottle in an argon atmosphere. This solution was standardized against a solution of potassium hydrogen phthalate using the derivative method with reproducibility of 0.001. *Mercury oxide, potassium iodide* and *potassium chloride,* p.a., Lachema Brno, were not further purified. *Twice-redistilled water* kept for 50 min prior to that in a sonographic bath was used in the preparation of solutions.

2.2 Apparatus and pH-Spectrophotometric Titration Procedure

The used apparatus and titration procedures were described in detail previously [34–38]. The free hydrogen-ion concentration $[H^+]$ was measured on a digital voltmeter Hanna HI 3220 with a precision of ± 0.002 pH units using a combined glass electrode Theta HC 103-VFR. The potentiometric titrations of the drug with potassium hydroxide were performed using the hydrogen activity scale. Standardization of the pH meter was performed using WTW standard buffers values 4.006 (4.024), 6.865 (6.841) and 9.180 (9.088) at 25 °C and 37 °C, respectively, in parentheses.

The spectrophotometric multiple-wavelength pH-titration was carried out as follows: 20.00 cm^3 of an aqueous solution containing 10^{-4} $mol{\cdot}L^{-1}$ drug, 0.100 $mol{\cdot}L^{-1}$ hydrochloric acid and 10 cm^3 indifferent solution KCl for adjustment of ionic strength was titrated with standard 1.0 $mol{\cdot}dm^{-1}$ KOH at 25 °C and 37 °C, respectively, and 80 absorption spectra were recorded. Titrations were performed in a water-jacketed double-walled glass vessel of 100 mL, closed with a Teflon bung containing the electrodes, an argon inlet, a thermometer, a propeller stirrer and a capillary tip from a micro-burette. All pH measurements were carried out at 25.0 ± 0.1 °C and 37.0 ± 0.1 °C. When the drug was being titrated, a stream of argon gas was bubbled through the solution both for stirring and for maintaining an inert atmosphere. The argon was first passed through an aqueous ionic medium by prior passage through one or two vessels also containing some of the titrand medium before entering the corresponding titrand solution. The burettes used were syringe micro-burettes of 1250 µL capacity (META, Brno) with a 25.00 cm micrometer screw [34]. The polyethylene capillary tip of the micro-burette was immersed into the solution when adding reagent solution but pulled out after each addition in order to avoid leakage of the reagent during the pH read out. The micro-burette was calibrated by ten replicate determinations of the total volume of delivered water by weighing on a Sartorius 1712 MP8 balance with results evaluated statistically, leading to a precision of $\pm 0.015\%$ in added volume over the whole volume range. The solution was pumped into the cuvette and spectrophotometric measurements were performed with the use of a Cintra 40 (GBC, Australia) spectrophotometer.

2.3 Software Used

An estimation of the dissociation constants was performed by the nonlinear regression analysis of the UV-metric spectra analysis using the SQUAD84 [21] and REACTLAB [39] programs and potentiometric pH-metric titration data using the ESAB program [13, 14], and by spectra interpretation using the INDICES program [40]. Most graphs were plotted using ORIGIN 9.1, Ref. [41] ACD/Percepta [23–29], and MARVIN [25, 26, 28, 30–33],

and PALLAS [26, 42] programs for predictions of pK_a values are based on the structural formulae of the drug compounds.

3 Computational Proceedure

A detailed tutorial of UV/VIS pH-titration method [36], also called the *UV-metric spectra analysis* [19], and alternatively the *pH-metric analysis* has been applied [35, 36, 38, 43–45]. Both instrumental methods can be used not only to determine the dissociation constants pK_a, but also the standard state enthalpy $\Delta H°$, entropy $\Delta S°$ and Gibbs energy $\Delta G°$ of reaction, even for sparingly soluble drugs. An investigation into the entropic and enthalpic properties of the dissociation process of drugs in water is very important for correct understanding their acidic behavior [46–50]. The concept of QSAR/QSPR [8] is used to transform searches for compounds with desired properties using chemical intuition and experience into a mathematically quantified and computerized form. The energy of protonation, defined as the difference between the total energies of the protonated and neutral forms of a molecule, can be considered to be a good measure of the strength of hydrogen bonds (the higher the energy, the stronger the bond) and can be used to determine the correct localization of the most favorable hydrogen bond acceptor site [51–54]. Changes in the Gibbs energy, enthalpy and entropy are *thermodynamic parameters.* Relationships between these thermodynamic parameters for a series of reactions are termed '*extrathermodynamics*' [8]. These extrathermodynamics are all relationships that are approximate and statistical, rather than strictly valid or mathematical. For example, a linear relationship between the entropy change ΔS and enthalpy ΔH has been observed in a variety of processes of small solutes in aqueous solutions. Enthalpy–entropy compensation has been a widely observed effect in physical, biological, chemical and biochemical processes [55–59] and is excellently reviewed by Liu and Guo [60]. It has been observed that as long as some conditions such as pH, solvent composition, a reactant molecule, water activity, ionic hydration [61], hydrogen bonding [62], etc. is changed, the enthalpy and entropy of activation change accordingly. Stronger intermolecular interaction or bonding (related to the enthalpy) will lead to a greater reduction of the configurational freedom, and hence greater order of the system (related to the entropy) [60]. The existence of a linear relationship between enthalpy ($\Delta H°$) and entropy ($\Delta S°$) of activation indicates compensation, and the equations are expressed as $\Delta H° = \text{slope} \cdot \Delta S° + \text{intercept}$. Although enthalpy–entropy compensation has in the past been regarded as a "ubiquitous property of water" [63], it appears to be a property of all weak intermolecular interactions, of which hydrogen bonding in an aqueous solution is merely the one most frequently encountered in chemical, biochemical and supramolecular reactions [64]. Other details of the computational procedure are available in the supplementary material.

4 Results

The experimental and computation scheme to determine the dissociation constants of the multi-component system is taken from Meloun et al., *cf.* p. 226 in Ref. [65], and all steps are described in detail [36]. The methods of numerical analysis of pH-spectra and pH-potentiometric titration curves have proven to be the best instrumental methods because they reliably determine even close consecutive dissociation constants, even for poorly

soluble drugs. The spectroscopic pH titration (the UV-metric method) has been used as an alternative method to the potentiometric determination (the pH-metric method) of dissociation constants with large molar absorption coefficients due to its high sensitivity to the concentration of the substance, even at concentrations as low as 10^{-5} mol·L^{-1}. However, the investigated compound must contain chromophores in the vicinity of the ionization centers, and protonated and deprotonated species must exhibit a sufficient spectral difference. Nonlinear regression analysis of spectrophotometric data is therefore an efficient and reliable tool, even in the case of small changes in the pH–absorption spectrum.

4.1 UV-Metric Spectral Analysis

The experimental procedure and computational strategies for determination of dissociation constants by analyzing the pH-absorbance matrix were described in the 11 steps of the proposed procedure partly published previously in a Tutorial [36, 66, 67] and the first mention was also on p. 226 in Ref. [65]. In addition to determining the number of protonation equilibria, the number of differently protonated species, their relative concentration diagram and the graph of the molar absorption coefficients within the range of measured wavelengths, statistical reliability criteria along with reliability tests of the protonation model found, should be included. Prior to experimental determination, the first step of this analysis should be to familiarize itself with the structure of the molecule and its protonation centers, including the prediction of dissociation constants, based on a quantum-chemical calculation according to the structural formula of the molecule.

Step 1 Theoretically predicted pK_a *values of Nilotinib hydrochloride* The first step of data analysis was the prediction of dissociation constants, based on a quantum-chemical calculation and concerned with the structural pattern of the studied drug in Fig. 1. The prediction program MARVIN has identified six protonizable centers A, B, C, D, E and F for Nilotinib hydrochloride, which could be theoretically associated with up to five predicted dissociation constants (Fig. 2a). All six proton centers are located on nitrogen atoms. However, the electronic nature of the individual nitrogen atoms in a molecule differ considerably, as it is influenced by various electronic and steric effects. To facilitate the interpretation of the ionization centers of the molecule and the prediction of dissociation constants, the Nilotinib hydrochloride molecule was subdivided into four suitable fragments. These fragments represent similar molecules that could be considered as simplified portions of Nilotinib hydrochloride with protonation centers A, B, C, D, E and F. However, the fragment containing similar protonation centers was not affected by the electron field of the rest of the molecule, and therefore its predicted dissociation constant may differ from those predicted for the entire Nilotinib hydrochloride molecule. The prediction programs MARVIN, PALLAS and ACD/Percepta predicted slightly different dissociation constants, so it was obvious that an experimental determination would be expected to be more reliable. The MARVIN program also presented a distribution diagram of all the theoretically predicted protonated Nilotinib hydrochloride species (Fig. 2b). It predicted up to 100% of the representation of the species, namely the anion L^- in dissociation of the D position at pH 12–14, the neutral molecule at pH 6–12, the cation LH^+ in protonation of position B or C at pH 2–6, cation LH_2^{2+} in protonation of positions B, D, E, C at pH 0–3, and finally cation the LH_3^{3+} in protonation of position A, B, C, D, E at pH 0–2.

Step 2 The number of light-absorbing species n_c The Cattel index graph of eigenvalues (Fig. 3) showed that the entire set of spectra of Nilotinib hydrochloride at the wavelengths of 220–320 nm was able to indicate three light-absorbing species in the mixtures,

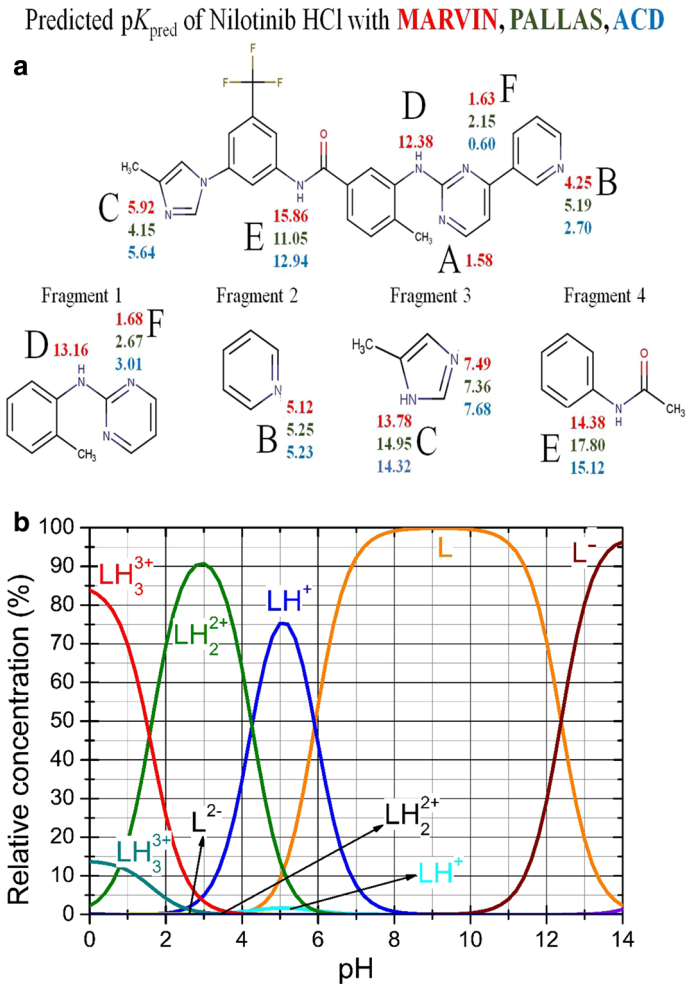

Fig. 2 *Graph* ***a*** molecular structure of Nilotinib hydrochloride (insert) with highlighted protonation centers **A**–**F**, and predicted pK_a values using the MARVIN, PALLAS and ACD/Percepta programs. Structure of auxiliary fragments 1–4 and their predicted pK_a values. *Graph* ***b*** the distribution diagram of the relative concentrations (%) of variously protonated ions of Nilotinib hydrochloride for predicted dissociation constants

$n_c = k^* = 3$ and $s_{inst}(A) = 1.0$ mAU, because the spectra of the molar absorption coefficients of the first pair of cations LH^+ and LiH_2^{2+} were very similar and the spectra of the second pair of cations LH_3^{3+} and LH_4^{3+} were also the same. Thus, factor analysis was unable to distinguish the true number of light absorbing species from the spectral noise, although this task could be correctly evaluated through non-linear regression analysis. These conclusions were also confirmed by Fig. 5, which showed that there were two pairs of very similar spectra of molar absorption coefficients of cations LH^+ and LH_2^{2+} and cations LH_3^{3+} and LH_4^{4+}. The difference in spectra of these species in each pair is nearly that of the noise level in the measured absorbance.

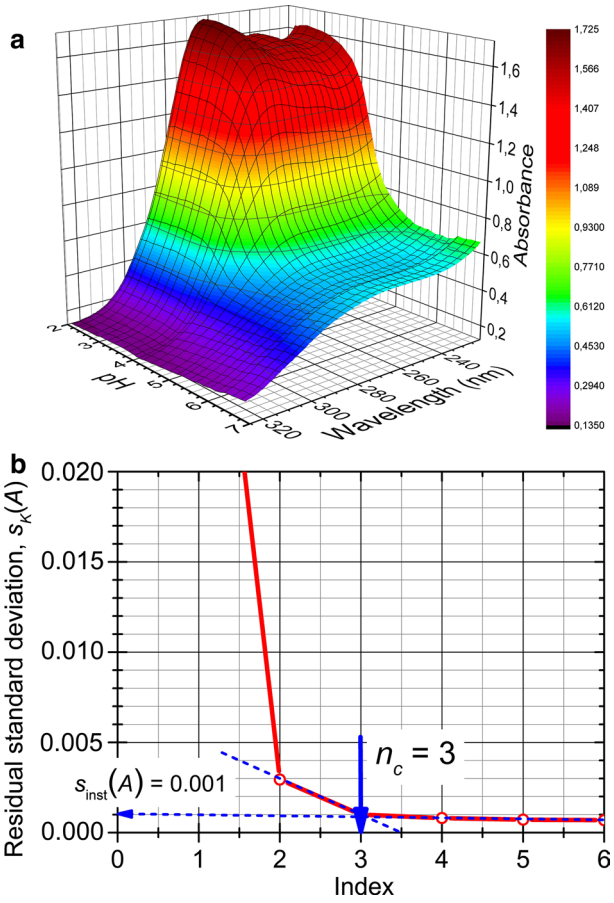

Fig. 3 *Graph **a*** the absorbance response surface of Nilotinib hydrochloride as dependent on pH. *Graph **b*** using the Cattel index graph with the residual standard deviation $s_k(A)$, the rank of the absorbance matrix is $k^* = 3$ for Nilotinib hydrochloride or the number of species is equal to $n_c = 3$. (INDICES in S-PLUS) [42]

Step 3 Diagnostics of the protonation model building and testing In both programs, REACTLAB [39] and SQUAD84 [21, 68], nonlinear regression analysis was used in the data treatment, *i.e.* the regression triplet method (data critique, model critique and method critique), cf. Ref. [43–45]. Finding the best hypothesis of a protonation model containing two, three or four dissociation constants is shown in the graphs of the molar absorption coefficients and the distribution diagrams of all the differently protonated species for the three proposed hypotheses of the protonation model (Fig. 4).

The design and building of the protonation model is the decision-making process for accepting the calculated parameters with some statistical diagnostics for the proposed hypothesis of the protonation model (Table 1). The hypothesis of the protonation model is the starting point of the iterative minimization process of the residual-square-sum function, *RSS*. Usually, all of the above diagnostics should be taken into consideration because none of them alone can be taken as a sufficiently reliable indicator of the success of the estimation or its failure. It was thus shown that the building of the Nilotinib hydrochloride protonation model is not an easy task because this drug has very close consecutive dissociation constants ($\left| pK_{ai} - pK_{ai+1} \right| < 3$) and, in addition, the pH slightly affected the changes in the absorbance values of chromophores in the spectra. Often, it can happen that the minimization process fails or is divergent. The failure of

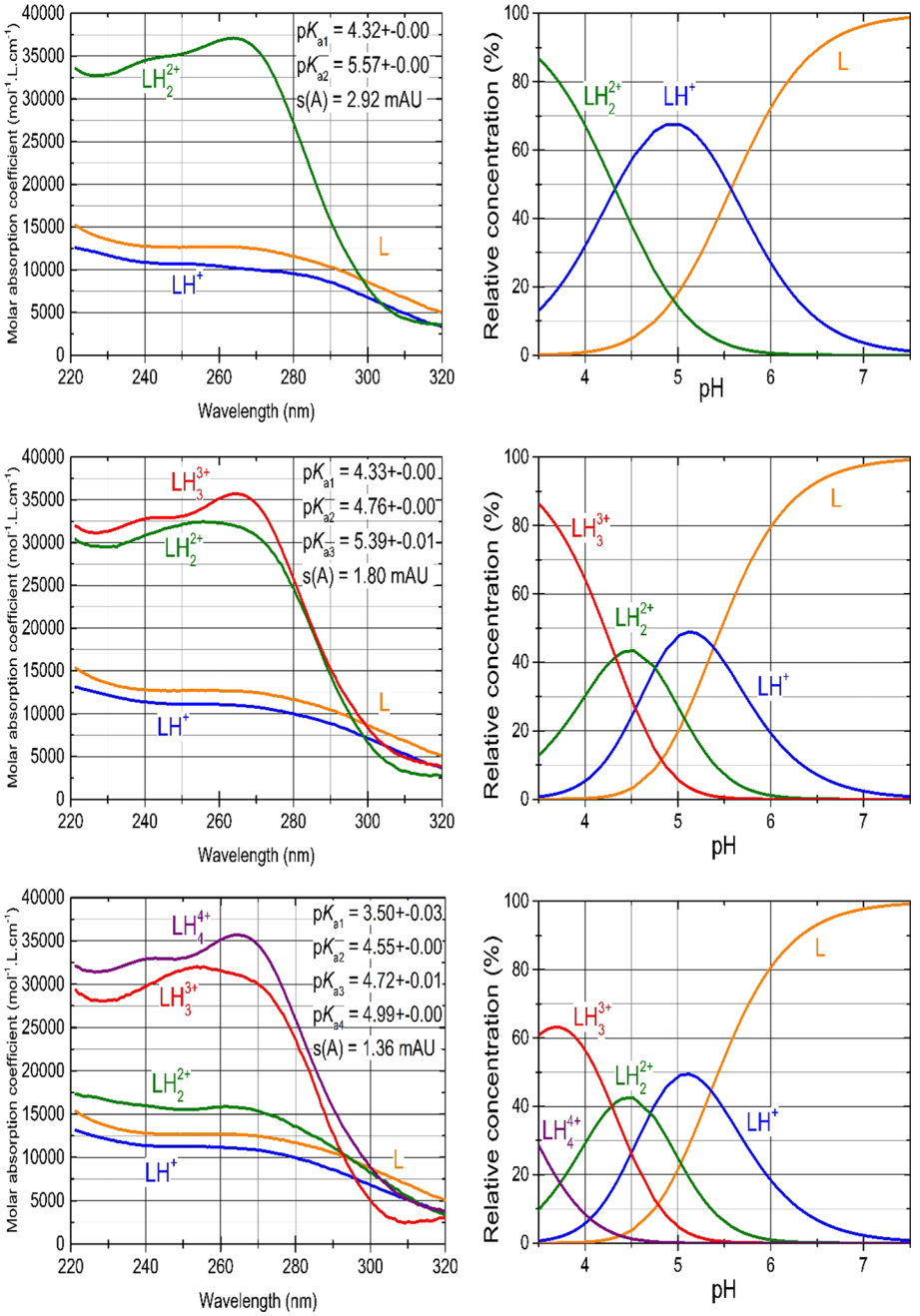

Fig. 4 Building and testing of the best protonation model of Nilotinib hydrochloride in the pH range of 2 to 7 for two (upper 2 graphs), three (middle 2 graphs) and four (lower 2 graphs) dissociation constants pK_{a1}, pK_{a2}, pK_{a3}, and pK_{a4} with the spectra analysis of 1.0×10^{-4} mol·L^{-1} Nilotinib hydrochloride at $I=0.0026$ mol·L^{-1} and 25 °C. Left graphs: pure spectral profiles of molar absorption coefficients versus wavelength (nm) for all the variously protonated ions of Nilotinib hydrochloride. Right graphs: The distribution diagram of the relative concentrations of all of the variously protonated species as dependent on pH (REACTLAB, ORIGIN 9)

Table 1 The reproducibility of the best protonation model of Nilotinib hydrochloride in the pH range from 3 to 7.5 with four dissociation constants pK_{a1}, pK_{a2}, pK_{a3}, and pK_{a4} using SQUAD84 and REACTLAB at 25 °C and 37 °C

Temperature		25 °C					37 °C				
Reproducibility		1st set	2nd set	3rd set	4rd set	Mean ± CID)	1st set	2nd set	3rd set	4rd set	Mean ± CI
Cattel's scree plot indicating the rank of the absorbance matrix (INDICES)											
Number of spectra measured, n_s		33	29	28	30		26	23	33	31	
Number of wavelengths, n_w		83	82	82	82		82	81	81	82	
Number of light-absorbing species, k^*		3	3	3	3		3	3	3	3	
Residual standard deviation, $s_k^*(A)$ (mAU)		0.66	0.64	0.84	0.85		1.02	1.12	1.06	0.75	
Estimates of dissociation constants in the searched protonation model											
pK_{a1} (s_1): $LH_4^{4+} \rightleftharpoons H^+ + LH_3^{3+}$	SQUAD84	3.57 (04)	3.92 (00)	3.50 (02)	3.41 (03)	3.66 ± 0.28	3.72 (03)	3.79 (01)	3.55 (04)	3.42 (06)	3.61 ± 0.20
	REACTLAB	3.59 (04)	3.59 (02)	3.50 (03)	3.59 (02)	3.55 ± 0.06	3.89 (01)	3.85 (01)	3.89 (01)	3.81 (01)	3.86 ± 0.05
pK_{a2} (s_2): $LH_3^{3+} \rightleftharpoons H^+ + LH_2^{2+}$	SQUAD84	4.53 (00)	4.17 (00)	4.46 (00)	4.78 (00)	4.47 ± 0.34	4.36 (00)	4.49 (00)	4.44 (00)	4.13 (02)	4.31 ± 0.20
	REACTLAB	4.53 (01)	4.51 (00)	4.55 (00)	4.59 (01)	4.55 ± 0.04	4.38 (00)	4.43 (00)	4.43 (01)	4.35 (01)	4.39 ± 0.05
pK_{a3} (s_3): $LH_2^{2+} \rightleftharpoons H^+ + LH^+$	SQUAD84	4.74 (00)	4.75 (00)	4.80 (00)	4.68 (00)	4.74 ± 0.06	4.71 (00)	4.60 (01)	4.68 (00)	4.99 (03)	4.79 ± 0.21
	REACTLAB	4.73 (00)	4.75 (01)	4.72 (01)	4.68 (00)	4.72 ± 0.04	4.72 (01)	4.77 (01)	4.68 (03)	4.75 (00)	4.73 ± 0.05
pK_{a4} (s_4): $LH^+ \rightleftharpoons H^+ + L$	SQUAD84	4.99 (00)	4.99 (01)	4.99 (00)	5.01 (00)	5.00 ± 0.01	5.29 (00)	5.33 (00)	5.30 (00)	5.31 (01)	5.31 ± 0.02
	REACTLAB	4.98 (00)	4.99 (00)	4.99 (00)	5.01 (00)	4.99 ± 0.01	5.27 (00)	5.33 (00)	5.31 (01)	5.36 (00)	5.31 ± 0.05
Goodness-of-fit test with the statistical analysis of residuals											
Mean residual $E\left\vert \bar{e} \right\vert$ (mAU)	SQUAD84	0.79	0.91	1.07	0.84		0.79	1.09	0.95	0.89	
	REACTLAB	0.79	0.91	0.98	0.78		0.79	1.12	0.96	1.08	
Standard deviation of residuals $s(\hat{e})$ (mAU)	SQUAD84	1.08	1.29	1.58	1.15		1.09	1.56	1.32	1.28	
	REACTLAB	1.01	1.17	1.34	0.98		0.99	1.45	1.24	1.42	
Sigma from ReactLab (mAU)	REACTLAB	1.02	1.20	1.36	1.00		1.01	1.48	1.29	1.44	
Hamilton R-factor from SQUAD84 (%)	SQUAD84	0.27	0.29	0.37	0.32		0.25	0.32	0.31	0.31	

Solutions of 1×10^{-4} mol·L^{-1} Nilotinib at $I = 0.002$ mol·L^{-1} and 25 °C, 37 °C were used for n_s spectra measured at n_w wavelengths. The standard deviations of the parameter estimates are in the last valid digits in parentheses. The resolution criterion and reliability of parameter estimates found are proven with goodness-of-fit statistics such as the residual standard deviation by factor analysis $s_k(A)$ (mAU), the mean residual $E\left\vert \bar{e} \right\vert$ (mAU), the standard deviation of absorbance after termination of the regression process $s(\hat{e})$ (mAU), the sigma $s(A)$ (mAU) from REACTLAB and the Hamilton R-factor of relative fitness [%] from SQUAD84 and the confidence interval of the mean ± CI

the parameter estimation refinement process mainly occurs in cases where the species was not present in sufficiently high concentration or when the pK_{ai} of the i-species was highly correlated with the pK_{ai+1} of the other $(i+1)$-species; these species would have the similar effect on pH. This occurred exactly in our case of three very close dissociation constants pK_{a1}, pK_{a2} and pK_{a3}. Such dissociation constants are then ill-conditioned in a regression model and their determination is difficult and often quite impossible. The ill-conditioned dissociation constants also were manifested by the large variance of replicate values and therefore by somewhat large standard deviations. There might also be a case where refinement of the dissociation constants estimates was successful, but one or more standard deviations are too "large". Then, after the statistical significance test, the dissociation constant estimate might not differ significantly from zero. In addition to the frequently used Student t test of the statistical significance of the pK_{ai} parameter, the literature also states an empirical rule according to Sillén that for a quality estimate pK_{ai}, the inequality $F \times s(pK_{ai}) < pK_{ai}$ should be applied.

For the initial (zero order) approximation of an estimation of the dissociation constants pK_{ai} for such a complicated equilibria task, the minimization process should not be completely wrong or very far from the true value.

When the minimization process fails or a divergence occurs, the numerical shift in minimization process of the parameters estimation is reduced to finding such a set of parameter estimates that gives a lower sum of squares.

A test of the best hypothesis criterion is the fitness test of the calculated spectra by the experimental points of the absorbance matrix, often simplified to quantifying the standard deviation of the absorbance after a regression termination, $s(A) = \sqrt{RSS/(n-m)}$, where n is the number of experimental points and m is the number of estimated parameters. The best curve fitting on Fig. 4 was achieved with the standard deviation of absorbance after regression termination $s(A) = 1.36$ mAU for the hypothesis of the four dissociation constants and five differently protonated species L, LH^+, LH_2^{2+}, LH_3^{3+}, and LH_4^{4+}, although the spectra of some pairs of species are similar or nearly the same.

In Table 1 the numerical estimates of dissociation constants, computed by two regression programs, SQUAD84 and REACTLAB, are compared: the residual mean $E|e|$ (mAU) or the median (mAU), residual standard deviation $s(e)$ (mAU) and Hamilton *R-factor* of relative fitness (%) from SQUAD84 showed that an excellent goodness-of-fit of calculated spectra through experimental points of all spectra was achieved for the protonation model with four dissociation constants. It can be argued that REACTLAB always offers more reliable parameter estimates as it achieves better fitting spectra than the older SQUAD84 program with the classical Newton–Raphson method used in minimization. Reliability of calculated estimates of regression parameters can be advantageously tested by the following regression diagnostics (Table 1 and Fig. 4) as explained in detail on p. 226 in Ref. [65].

(a) *Physical significance of parameter estimates* In the left part of Fig. 4, the spectra of the molar absorption coefficients ε_L, ε_{LH}, ε_{LH2}, ε_{LH3}, and ε_{LH4} of all the differently protonate sprcies of Nilotinib hydrochloride species versus wavelengths are shown. The pair of ε_{LH3} and ε_{LH4} curves, as well as the ε_L and ε_{LH} pairs, seem to be close and almost the same. The model with four pK_a values better represented the measured spectra and achieved a closer fitting.

(b) *Physical significance of species concentrations* The distribution diagram of the relative concentrations of all species (Fig. 4) shows the protonation equilibria of the differently

protonated species L, LH^+, LH_2^{2+}, LH_3^{3+}, and LH_4^{4+}. The graph shows that none of the species is a minor one, all of which are of physical significance.

(c) *The goodness-of-fit test* Although statistical analysis of residuals on p. 101 in Ref. [65] represents one of the most reliable tests of estimated regression parameters, some empirical physico-chemical limitations need to be taken into account. The statistical measures of all residuals showed that the pit of the elliptic hyperparaboloid of the objective *RSS* function (Table 1) had reached its minimum. In goodness-of-fit test the residual mean $E\left|\bar{e}\right|$ (mAU) and the residual standard deviation $s(\hat{e})$ (mAU) reached very low values of less than 2 mAU, representing less than 0.2% of the measured absorbance value. Good spectra fitting was also confirmed by the low value of the Hamilton *R-factor*, which was usually less than 0.5%. The median reached a low value near zero.

Step 4 The effective range of wavelengths Three ranges of wavelengths 220–320 nm, 280–320 nm and 220–280 nm were selected and the spectra for these wavelength ranges were evaluated. Figure 5 illustrates the estimates of four dissociation constants including the quality of curve fitting expressed here with the standard deviation of absorbance $s(A)$, which serves here as a reliability criterion of the calculated parameter estimates. The best curve fitting with the fitting criterion $s(A) = 1.36$ mAU was achieved in the wavelength range 220–320 nm, although the estimates of the dissociation constants were close in all three tested wavelength ranges. Likewise, the four distribution diagrams of the relative concentration of variously protonated species in Fig. 5 are quite similar.

Step 5 The absorbance change in spectra within pH titration Adjustment and change of pH did not cause significant changes everywhere in the Nilotinib hydrochloride spectrum, because some chromophores were only slightly affected by pH adjustment. Figure 6a shows a spectrum of molar absorption coefficients, depending on the wavelength, for six selected wavelengths A through F, for which the A versus pH curves are displayed. Figure 6b shows a distribution diagram of the relative concentrations of all five differently protonated species, which indicates all consecutive protonation equilibria with close dissociation constants. The plots **A**–**F** show the sensitivity of chromophores in the Nilotinib hydrochloride molecule on the pH, which was monitored in the form of A versus pH curves. The maximum change in absorbance occurs at 220–270 nm for pH changes of pH 3 to 6 (curves **A**, **B** and **C**) with minor changes in absorbance in the wavelength range 300–370 nm for pH 5.5 to 8 (curves **D**, **E** and **F**). The graphs show estimates of dissociation constants and the presence of predominant differently protonated species. From these graphs it was also clear that the first three dissociation constants are very close and that therefore their estimation will be difficult or sometimes even impossible to evaluate. Each of the **A**–**F** graphs in Fig. 6 also contain a plot of residuals. The quality of residuals reveals the degree of curve fitness of the calculated A versus pH curve through the experimental absorbance points. The residuals should oscillate around zero and their $\pm$ signs should change with their frequent oscillations. The residuals should also exhibit a Gaussian distribution with a mean value or with a median equal nearly to zero. The standard deviation is expected to be of the same size as the instrumental noise in absorbance, $s_{inst}(A)$.

Step 6 The signal-to-error ratio in spectra changes In the spectrophotometric determination of pK_a of Nilotinib hydrochloride, it was first necessary to investigate whether the adjustment of pH would cause a sufficient absorbance change in spectrum. It is evident from Fig. 7a, b that the spectral response of the chromophore Nilotinib hydrochloride molecule is not the same and sufficient for all four protonation equilibria, so it had

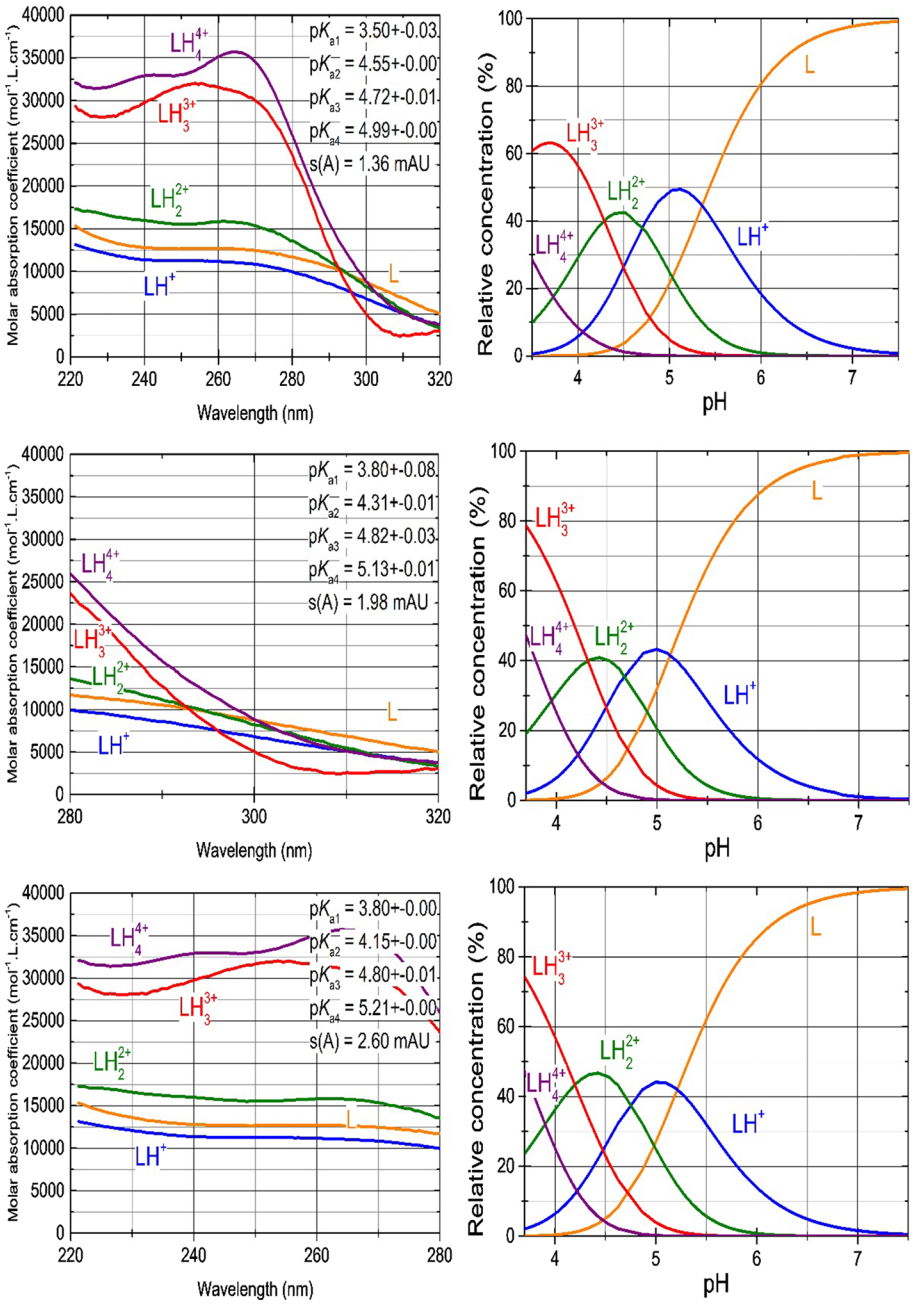

Fig. 5 Search for an effective wavelength range to examine the position of ionizable groups and chromophores to find a sufficient absorbance change in the spectrum for adjusted pHs, which allows a reliable determination of dissociation constants. The protonation model of four dissociation constants was analyzed using either the whole wavelength spectrum (upper 2 graphs) or by two separate absorption bands (middle and lower 2 graphs). The best-fitted spectra were achieved in the 220–320 nm range, although pK_a estimates were similar for all three wavelength ranges

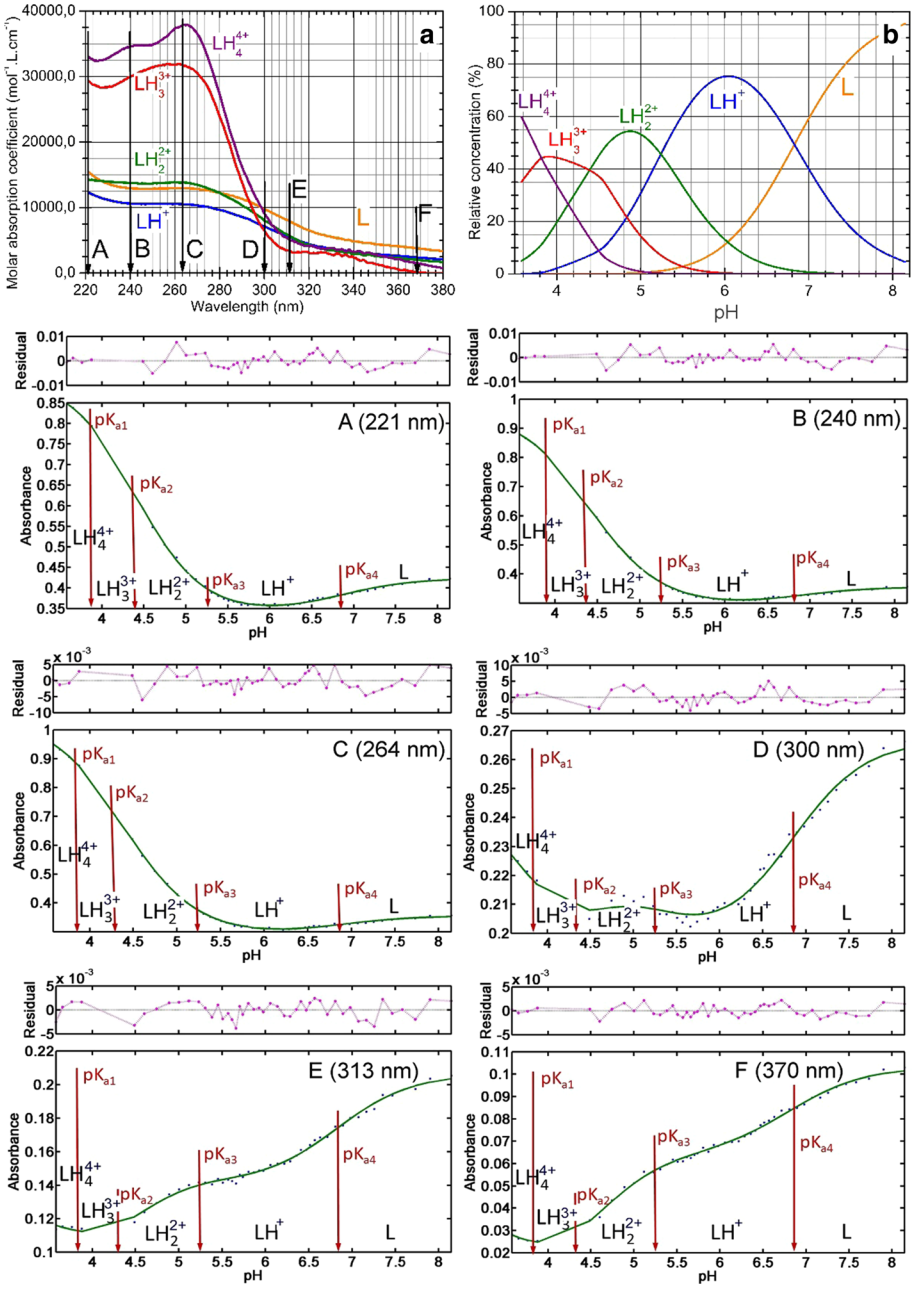

Fig. 6 The adjusted pH did not cause the same absorbance change in the Nilotinib hydrochloride spectrum because some chromophores were only slightly affected by the pH. Upper left graph: the spectrum of the molar absorption coefficient contains positions of six wavelengths **a** through **f** for which the *A* versus pH curves were analyzed. Upper right graph: the distribution diagram of the relative concentration of variously protonated species indicates a consecutive equilibrium with close dissociation constants. *Graphs **a** through **f***: the sensitivity of chromophores in the Nilotinib hydrochloride molecule to pH is analyzed

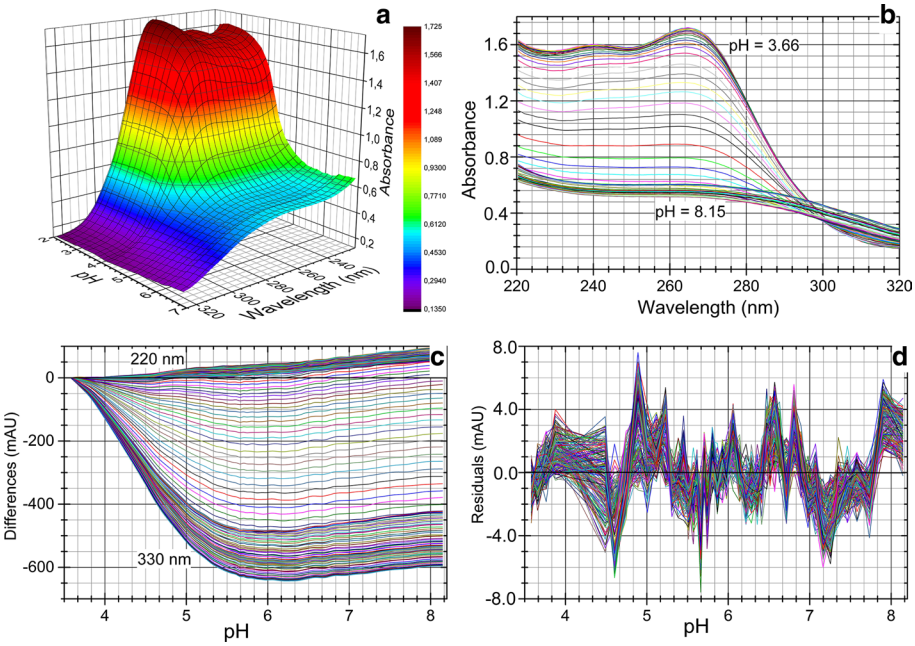

Fig. 7 Analysis of the change in absorbance spectra at adjusted pH. *Graph* ***a*** 3D-graph of the absorbance change in the Nilotinib hydrochloride spectrum upon pH-titration. *Graph* ***b*** 2D-graph of the absorbance change in the spectra set from $pH_1 = 3.66$ to $pH_n = 8.15$. *Graph* ***c*** the graph of the absorbance change differences D_{ij} (mAU) in the Nilotinib hydrochloride spectrum from 220 to 320 nm within pH titration. *Graph* ***d*** residuals ***e*** (mAU) show whether they were of the same size as the instrumental noise $s_{inst}(A)$ (REACTLAB, ORIGIN 9)

to be verified whether all four dissociation constants could be estimated even with such small changes in absorbance. The change for the *i*-th spectrum and the *j*-th spectrum absorption can be expressed by the relation $\Delta_{ij} = A_{ij} - A_i$ and then divided by the instrumental standard deviation $s_{inst}(A)$, resulting in a normalized change in the absorbance in spectrum, $SER = \Delta / s_{inst}(A)$, with A_i denoting the absorbance of the acid form of Nilotinib hydrochloride. It was necessary to investigate whether these small changes in absorbance Δ in the spectra were sufficiently large and mainly greater than the absorbance noise value, expressed by $s_{inst}(A)$.

The *SER* variations in the spectra were therefore plotted against the wavelength λ for all elements of the absorbance matrix (Fig. 7c) and showed that the absorbance changes were small, but that they were still larger than the instrumental noise or larger than the standardized residuals $e/s_{inst}(A)$ seen in Fig. 7d. While the values of $e/s_{inst}(A)$ are predominantly in the range of -4 to $+4$, the changes in *SER* are in the range of -650 to $+100$. However, smaller changes in absorbance in the spectra might cause a higher uncertainty of dissociation constants. According to the empirical rule that unless the *SER* is less than 10, the factor analysis in the program INDICES [54] might not correctly determine the number of light-absorbing species n_c and thus suggesting that changes in spectra were insufficient to determine dissociation constants.

Step 7 The spectra deconvolution The deconvolution of each experimental spectrum into the absorption bands of the individual species showed whether the protonation hypothesis

had been designed efficiently. In such areas of pH where there was a significant contribution of more species to the actual spectrum, it was then necessary to measure more spectra. Such a spectrum provides sufficient information for nonlinear regression analysis that monitored at least two species in equilibrium, but none of them should be a minor one. Figure 8 illustrates the deconvolution of six selected experimental spectra into absorption bands concerning differently protonated Nilotinib species. At pH 3.66, the absorption band of the cation LH_4^{4+}, which is in equilibrium with the cation LH_3^{3+}, and the cation $LH_2^{2=}$ spectrum is still insignificant. The pH range of 3.87 to pH 4.48 was very important, because there are three cations in equilibrium, namely LH_4^{4+}, LH_3^{3+} and LH_2^{2+}. At pH 5.62, the band of the cation LH^+ was increasing while the bands of LH_3^{3+} and LH_2^{2+} were decreasing. At pH 6.89 to pH 7.35, there were at least two species present in the solution, L and LH^+.

4.2 Analysis of pH-Metric Data

The potentiometric titration of the acidified Nilotinib hydrochloride with potassium hydroxide was carried out at 25 °C and 37 °C and at adjusted ionic strength (Fig. 9). In the analysis of pH-metric data, the initial estimate of each dissociation constant of Nilotinib hydrochloride was refined by the ESAB program.

Step 8 pH-metric data analyzed with the Bjerrum formation function Nilotinib hydrochloride has four dissociation constants and their refinement was carried out by the nonlinear regression of the pH-metric titration curve using the ESAB program. The nonlinear regression analysis was applied on the central part of the pH-metric titration curve for protonated acidified Nilotinib hydrochloride titrated with potassium hydroxide (Fig. 9). Estimates of four dissociation constants pK_{a1}, pK_{a2}, pK_{a3} and pK_{a4} were evaluated and plotted using the curve of the Bjerrum formation function. At a concentration higher than 3×10^{-4} mol·L^{-1}, a precipitate of Nilotinib hydrochloride was formed, which was first revealed by the slight opalescence of the fine precipitate.

Residuals are defined as the difference between the experimental and the calculated volume of the titrant KOH, $e_i = V_{\mathrm{exp},i} - V_{\mathrm{calc},i}$ (Table 2). The reliability test of the refined dissociation constants estimates was performed by the statistical analysis of residuals. By refining the *group parameters*, the statistics of a goodness-of-fit test significantly improved. The relatively sensitive reliability criterion of the estimated dissociation constants was the average of the absolute values of the residuals $\mathrm{E}\left|\bar{e}\right|$ (μL) and the median of residuals (μL). A comparison of the numerical value of this statistic with the instrumental noise represented here by the instrumental standard deviation of titrant KOH, $s_{\mathrm{inst}}(V) = s(V) = 0.1$ μL, has proven an excellent curve fitting, since the mean residual $\mathrm{E}\left|\bar{e}\right|$, median and the residual standard deviation of titrant KOH, $s(V)$, were equal or lower than the experimental noise, $s_{\mathrm{inst}}(V)$. The values of both monitored statistics here 0.1 μL were similar to the instrumental error of the used microburette $s(V) = 0.1$ μL. In addition, the residuals oscillate between the lower (−0.2 μL) and the upper limit (+0.2 μL) of the internal Hoaglin boundaries, and no residual value was found outside these limits (see p. 81, Ref. [69]). Estimates of dissociation constants refined by the program ESAB were therefore proven to be sufficiently reliable (Table 2). The curve fitting could be improved only by further refining the *group parameter* L_0, the concentration of the drug Nilotinib hydrochloride in the titration vessel.

Step 9 Uncertainty of pK_a *in replicate measurements* The reproducibility of the dissociation constants evaluated with two programs, SQUAD84 and REACTLAB, from four replicate measurements was found to be in good agreement from these two programs, as

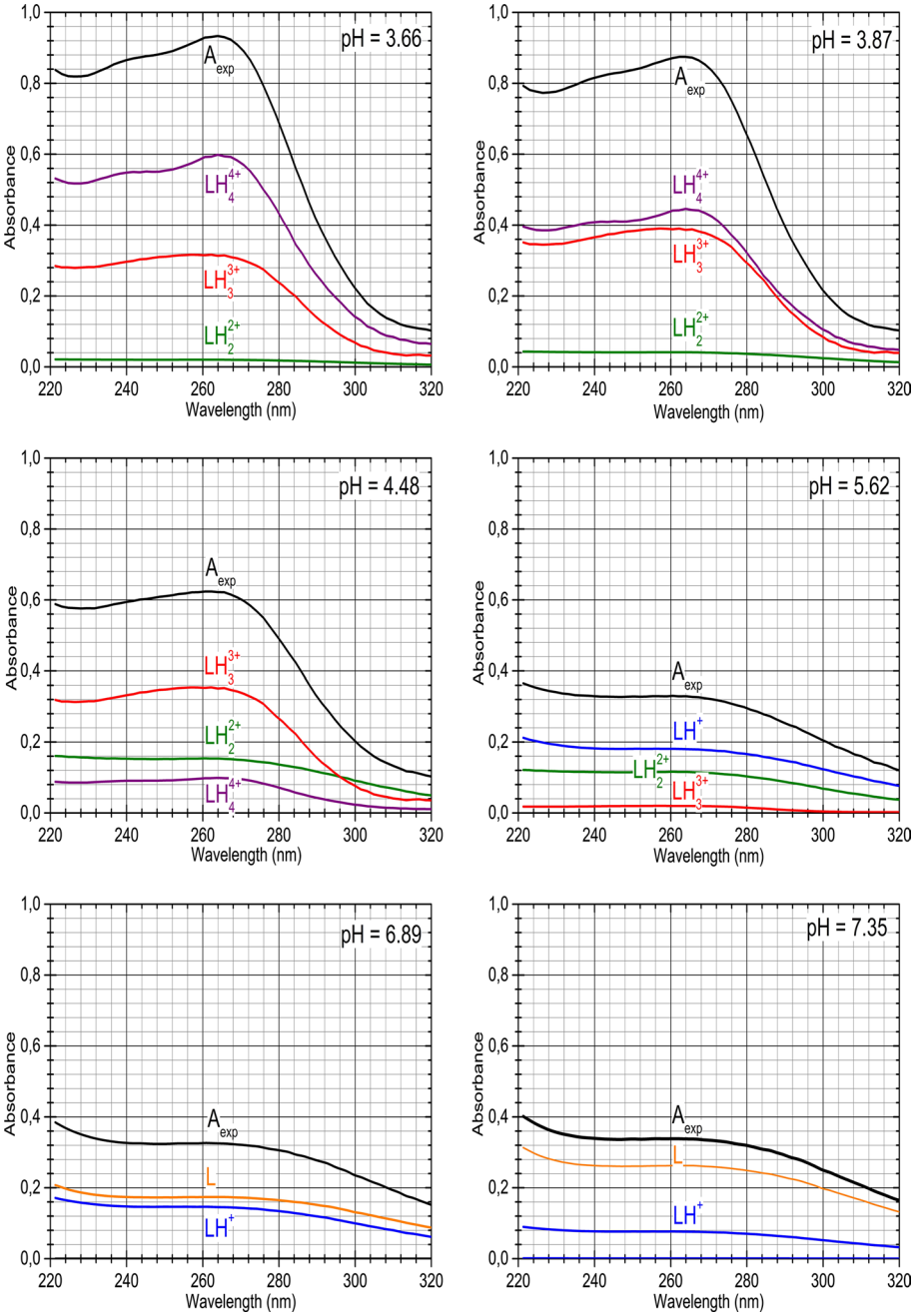

Fig. 8 Deconvolution of each experimental spectrum A_{exp} of 1.0×10^{-4} mol·L^{-1} Nilotinib hydrochloride at $I=0.0026$ mol·L^{-1} and 25 °C into the spectra of the individual differently protonated ions L, LH^+, LH_2^{2+}, LH_3^{3+}, and LH_4^{4+} in mixtures for pH 3.66, 3.87, 4.48, 5.62, 6.89, and 7.35 calculated by SQUAD84

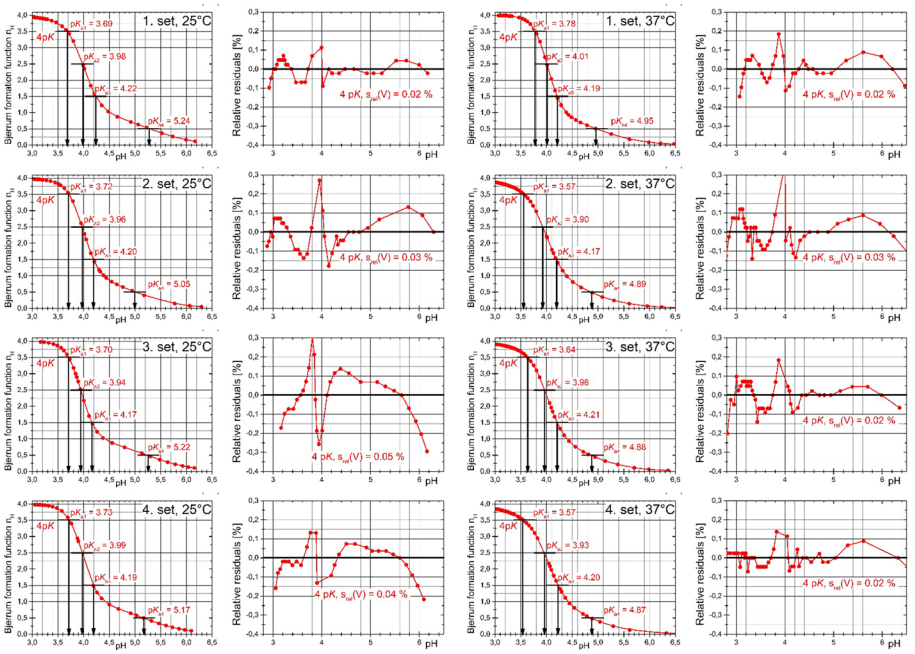

Fig. 9 Reproducibility in the search for the protonation model analyzing four pH potentiometric titration curves at 25 °C and 37 °C. Acidified Nilotinib hydrochloride was titrated with potassium hydroxide and the Bjerrum protonation curve was plotted for four dissociation constants, refined by the ESAB program. The residual graphs show that four dissociation constants led to the best curve fitting of titration curves (ESAB, ORIGIN)

is demonstrated in Table 1. The diagram on Fig. 10 shows that because, with an increasing temperature, the Nilotinib hydrochloride was better dissolved and so the dissociation constant estimates exhibited better reproducibility. However, Fig. 10 does not show good internal reproducibility of the $pK_{a,i}$ estimates, mainly at 25 °C. The interpretation is as follows:

(a) An interval estimate of the mean value from four repetitive dissociation constants also served here as a measure of uncertainty for each successive dissociation constant.
(b) At 25 °C the UV-metric method led to the one of the most precise estimates of the dissociation constant pK_{ai}, *i.e.* $pK_{a1} \pm 0.01$, while the $pK_{a4} \pm 0.02$ estimate was the most precisely estimated by the pH metric method.
(c) At 37 °C the UV-metric method exhibited the same precision of all four estimates, $pK_{ai} \pm 0.05$, while the $pK_{a2} \pm 0.02$ was the most precise value estimated by the pH-metric method.
(d) At 37 °C, the dissociation constant estimates were significantly more acidic, *i.e.*, they had lower values of pK_a than those estimates at 25 °C by the pH-metric method.
(e) Very close values of four consecutive dissociation constants could result in some difficulties in the minimization process or could make refinement failures in iterations. Reasons for this could be that an intermediate species was not present at a sufficiently high concentration for too close $pK_{a,i}$ values, or that the $pK_{a,i}$ value of one species was

Table 2 ESAB regression refinement of common and group parameters for a pH-metric titration of Nilotinib hydrochloride titrated with KOH at 25.0 °C and 37.0 °C and various adjusted ionic strength, the estimated dissociation constants pK_{a1}, pK_{a2}, pK_{a3} and pK_{a4} of Nilotinib hydrochloride where their standard deviations in the last valid digits are in parentheses

Temperature	25 °C				37 °C			
Total ionic strength ($mol{\cdot}L^{-1}$)	0.065	0.136	0.144	0.165	0.136	0.151	0.172	0.206
Estimates of the group parameters H_0, H_T and L_0 in the searched protonation model								
Number of points *n*	36	41	39	49	41	30	35	43
$H_0 \times 10^2$ ($mol{\cdot}L^{-1}$)	1.79 (00)	1.76 (00)	1.74 (00)	1.82 (00)	1.76 (00)	1.72 (00)	1.73 (00)	1.82 (00)
H_T ($mol{\cdot}L^{-1}$)	0.8139	0.8139	0.8139	0.8139	0.8139	0.8139	0.8139	0.8139
$L_0 \times 10^4$ ($mol{\cdot}L^{-1}$)	1.68 (00)	1.53 (00)	1.41 (00)	1.02 (00)	1.53 (00)	1.69 (00)	1.70 (00)	1.60 (00)
Estimates of the common parameters *i.e.* dissociation constants in the searched protonation model								
pK_{a1}	3.72 (01)	3.70 (01)	3.68 (02)	3.58 (06)	3.72 (08)	3.71 (01)	3.73 (02)	3.79 (02)
pK_{a2}	3.96 (01)	3.93 (01)	3.93 (02)	3.88 (06)	4.00 (07)	4.00 (01)	4.02 (02)	4.04 (02)
pK_{a3}	4.20 (01)	4.11 (01)	4.11 (02)	4.08 (06)	4.25 (07)	4.25 (01)	4.24 (02)	4.28 (02)
pK_{a4}	5.18 (01)	4.72 (04)	4.73 (05)	4.84 (13)	5.36 (16)	5.25 (04)	5.52 (11)	5.68 (09)
Goodness-of-fit test with the statistical analysis of residuals								
Bias or arithmetic mean of residuals $E(\hat{e})$ (µL)	6.25×10^{-3}	2.44×10^{-3}	-33.33×10^{-3}	-2.04×10^{-3}	-2.43×10^{-3}	3.33×10^{-3}	5.71×10^{-3}	2.33×10^{-3}
Median of residuals *M* (µL)	0.00	0.00	0.00	0.10	0.10	0.00	0.10	0.10
Mean of absolute value of residuals, $E\left\vert \hat{e} \right\vert$ (µL)	0.23	0.24	0.36	0.53	0.49	0.22	0.47	0.37
Residual standard deviation, $s(\hat{e})$ (µL)	0.28	0.37	0.43	0.70	0.62	0.28	0.62	0.48
Residual standard deviation, s_{rel}, (%)	0.17	0.04	−0.72	0.03	0.07	0.09	0.10	0.01
Residual skewness $g_1(\hat{e})$	−0.17	1.43	−0.02	−0.26	−0.12	0.36	0.10	−0.32
Residual kurtosis $g_2(\hat{e})$	1.88	6.44	2.50	3.48	2.91	3.10	3.25	3.47
Akaike-Information Criterion, *AIC*	−559.72	−643.23	−596.21	−704.31	−570.64	−483.89	−508.32	−651.12
Hamilton R-factor from ESAB (%)	0.08	0.08	0.10	0.16	0.07	0.06	0.07	0.10

The reliability of parameter estimation is proven with goodness-of-fit statistics: the bias or arithmetic mean of residuals $E(\hat{e})$ (µL), the median (µL), the mean of absolute value of residuals, $E\left\vert \hat{e} \right\vert$ (µL), the standard deviation of residuals $s(\hat{e})$ (µL), and the standard deviation of residuals $s_{rel}(\hat{e})$ (%), the residual skewness $g_1(\hat{e})$ and the residual kurtosis $g_2(\hat{e})$ proving a Gaussian distribution, the Hamilton R-factor of relative fitness [%] from ESAB and the Akaike-Information Criterion *AIC*. *Common parameters refined*: pK_{a1}, pK_{a2}, pK_{a3}, and pK_{a4}. *Group parameters refined*: H_0, H_T, and L_0. *Constants*: $t = 25.0$ °C, 37.0 °C, $pK_w = 13.9799$, $s(V) = s_{inst}(y) = 0.1$ µL, I_0 adjusted (in vessel), $I_T = 0.8139$ $mol{\cdot}L^{-1}$ (in burette KOH)

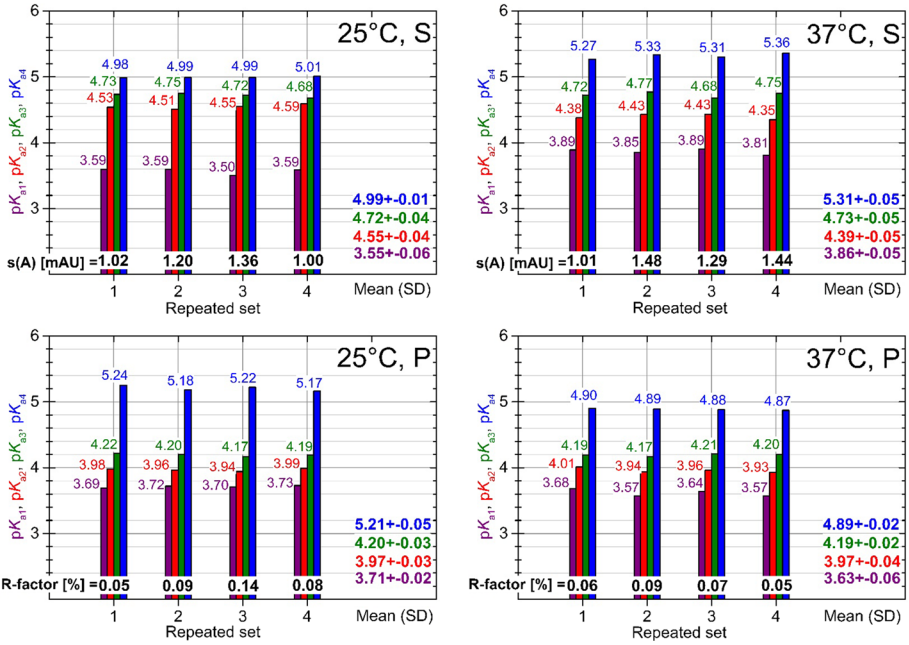

Fig. 10 The reproducibility of Nilotinib hydrochloride dissociation constants of the four replicate UV-metric measurements (*graph* 25 °C, ***S*** and *graph* 37 °C, ***S***) and four replicate pH-metric measurements (*graph* 25 °C, ***P*** and *graph* 37 °C, ***P***) are in agreement. Reproducibility of proton model estimates with four dissociation constants are compared. The arithmetic mean of dissociation constants with their confidence intervals were expressed on the basis of their standard deviation $s(A)$ and $s(V)$. Potentiometric pH-titration exhibited the better goodness-of-fit [67] (REACTLAB, SQUAD84, ESAB, ORIGIN 9)

highly correlated with the $pK_{a,i+1}$ value of another species so that those species would each have very similar effects on pH.

(f) One explanation could be that the starting initial value for one or more $pK_{a,i}$ could be far from their true value, or some aspect of the model could be wrong, as for example, if a species was missing, or its stoichiometry was wrong or there were not enough experimental data points to characterize a dissociation constant.

(g) When the normal equations are singular, one or more of the correlation coefficients between two parameters $pK_{a,i}$ are equal to one or minus one so that the refinement process could be terminated [16]. Such failure could be an indication of a serious mismatch between the model and the data, and therefore it was impossible to refine the $pK_{a,i}$ values.

(h) On the other hand, a refinement might terminate apparently successfully, but with one or more standard deviations $s(pK_{a,i})$ being labelled as "large". Generally, it should be noticed, that when the standard deviation $s(pK_{a,i})$ is large, the value of the dissociation constant, $pK_{a,i}$, might sometimes not be significantly different from zero.

Step 10 Thermodynamic dissociation constants By applying the Debye–Hückel equation to the data from Tables 1 and 2, the unknown parameter pK_{ai}^{T} was estimated at two temperatures of 25 °C and 37 °C. Because of the narrow temperasture range and also because of low ionic strength values, there could not be two parameters evaluated from the data,

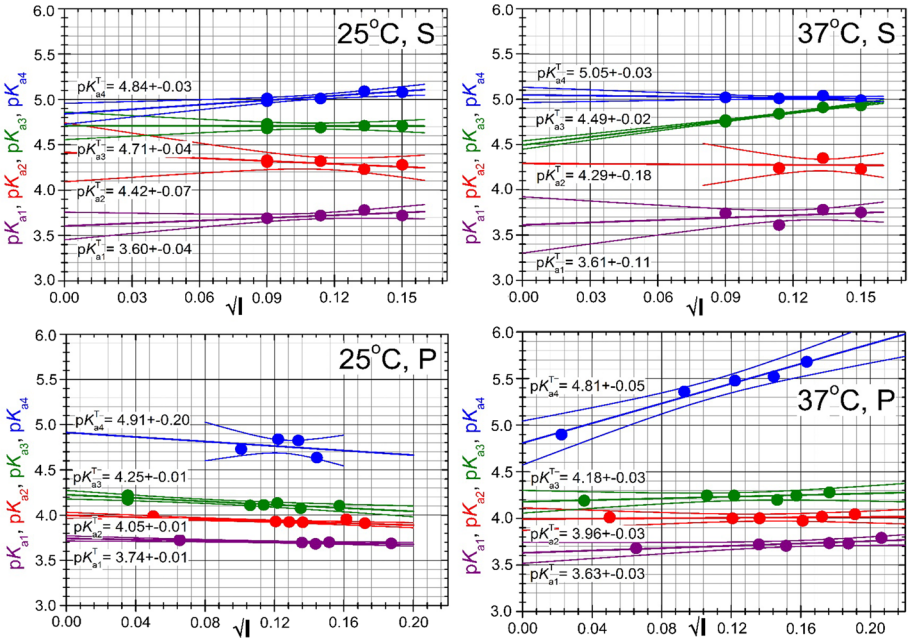

Fig. 11 Dependence of the mixed dissociation constants of Nilotinib hydrochloride on the square-root of the ionic strength for the four dissociation constants leading to the thermodynamic dissociation constants pK_{ai}^{T} using spectra analysis (*graph* 25 °C, ***S*** and *graph* 37 °C, ***S***) and the pH-metric technique (*graph* 25 °C, ***P*** and *graph* 37 °C, ***P***). The straight lines are drawn with the Working–Hotteling confidence bands (QCEXPERT)

namely the ion-size parameter *å* and the salting-out coefficient *C*, evaluated here. Figure 11 shows an extrapolation of the mixed dissociation constants to zero ionic strength according to the Debye–Hückel limiting law for the protonation model of four dissociation constants at 25 °C and 37 °C using linear straight lines with the Working–Hotteling 95% confidence bands, *cf*. p. 474 in Ref. [70]: $pK_{a1}^{T} = 3.60 \pm 0.04$, $pK_{a2}^{T} = 4.42 \pm 0.07$, $pK_{a3}^{T} = 4.71 \pm 0.04$, and $pK_{a4}^{T} = 4.84 \pm 0.03$ at 25 °C and $pK_{a1}^{T} = 3.61 \pm 0.11$, $pK_{a2}^{T} = 4.29 \pm 0.18$, $pK_{a3}^{T} = 4.49 \pm 0.02$, and $pK_{a4}^{T} = 5.05 \pm 0.03$ at 37 °C (spectrophotometrically) and $pK_{a1}^{T} = 3.74 \pm 0.01$, $pK_{a2}^{T} = 4.05 \pm 0.01$, $pK_{a3}^{T} = 4.25 \pm 0.01$, and $pK_{a4}^{T} = 4.91 \pm 0.20$ at 25 °C and $pK_{a1}^{T} = 3.63 \pm 0.03$, $pK_{a2}^{T} = 3.96 \pm 0.03$, $pK_{a3}^{T} = 4.18 \pm 0.03$, and $pK_{a4}^{T} = 4.81 \pm 0.05$ at 37 °C (potentiometrically). Broader confidence bands show a higher uncertainty of estimated dissociation constants in the UV-metric spectra analysis for pK_{a2} at both temperatures 25 °C and 37 °C and in pH-metric analysis for pK_{a4}, also at both temperatures 25 °C and 37 °C.

Step 11 Determination of enthalpy, entropy and Gibbs energy for the „extra-thermodynamics" of dissociation The enthalpy change $\Delta H°$ of the dissociation process was calculated from the van't Hoff equation $\mathrm{d}\ln K/\mathrm{d}T = \Delta H°/RT^2$. From the values of Gibbs energy $\Delta G° = -RT \ln K$ and enthalpy $\Delta H°$, the entropy $\Delta S° = (\Delta H° - \Delta G°)/T$ can be calculated, where R (ideal gas constant) = 8.31451 $\mathrm{J{\cdot}K^{-1}{\cdot}mol^{-1}}$, K is the thermodynamic dissociation constant and T is the absolute temperature.

Positive enthalpy values $\Delta H°$ (pK_{a1}) = 16.23 $\mathrm{kJ{\cdot}mol^{-1}}$, $\Delta H°$ (pK_{a2}) = 13.28 $\mathrm{kJ{\cdot}mol^{-1}}$, $\Delta H°$ (pK_{a3}) = 10.33 $\mathrm{kJ{\cdot}mol^{-1}}$, and $\Delta H°$ (pK_{a4}) = 14.75 $\mathrm{kJ{\cdot}mol^{-1}}$ at 25 °C showed that the dissociation process is endothermic and was accompanied by absorption of heat. Positive

values of the Gibbs energy $\Delta G°$ (pK_{a1}) = 21.35 and 20.72 kJ·mol^{-1}, $\Delta G°$ (pK_{a2}) = 23.12 and 22.60 kJ·mol^{-1}, $\Delta G°$ (pK_{a3}) = 24.26 and 23.86 kJ·mol^{-1}, and $\Delta G°$ (pK_{a4}) = 28.02 and 27.45 kJ·mol^{-1} at 25 °C and 37 °C, respectively, indicated that the dissociation process did not proceed spontaneously. As the entropy of dissociation $\Delta S°$ (pK_{a1}) = − 0.017 and − 0.015 kJ·K^{-1}·mol^{-1}, $\Delta S°$ (pK_{a2}) = − 0.033 and − 0.030 kJ·K^{-1}·mol^{-1}, $\Delta S°$ (pK_{a3}) = − 0.047 and − 0.044 kJ·K^{-1}·mol^{-1}, $\Delta S°$ (pK_{a4}) = − 0.045 and − 0.041 kJ·K^{-1}·mol^{-1} at 25 °C and 37 °C, respectively, are negative, the dissociation process was reversible.

Thermodynamic parameters of 89 dissociation constants for 44 drug acids and bases were published [8] in order to predict the extent of these dissociation reactions and the position of equilibrium for processes in which these reactions occur. Using the original set of 89 data points, the orthogonal least-squares algorithm found the two regression parameters estimates, the intercept a and the slope b, of the linear dependence in which both variables appear to be strongly correlated according to the regression equations forming straight lines in Fig. 12 shown with different colors: *graph* ***a***: $\Delta H° = a + b \cdot pK_a$, *graph* ***b***: $T\ \Delta S° = \Delta H° + b \cdot RT\ \ln\ K_a$, *graph* ***c***: $\Delta H° = \Delta G° + b \cdot T\ \Delta S°$, and *graph* ***d***: $\Delta G° = -T\ \Delta S° + b \cdot \Delta H°$ (Fig. 12a–d). Each graph in Fig. 12 represents the regression model and the graph of the four straight lines concerning the cations LH^+, LH_2^{2+}, LH_3^{3+} and LH_4^{4+} for the prediction of the actual thermodynamics of Nilotinib (full circles). The experimentally evaluated thermodynamic properties are drawn here in triangles. When the experimental value of the thermodynamic parameter (triangle) is close to its predicted value (circle), it meants that its experimental determination was more reliable.

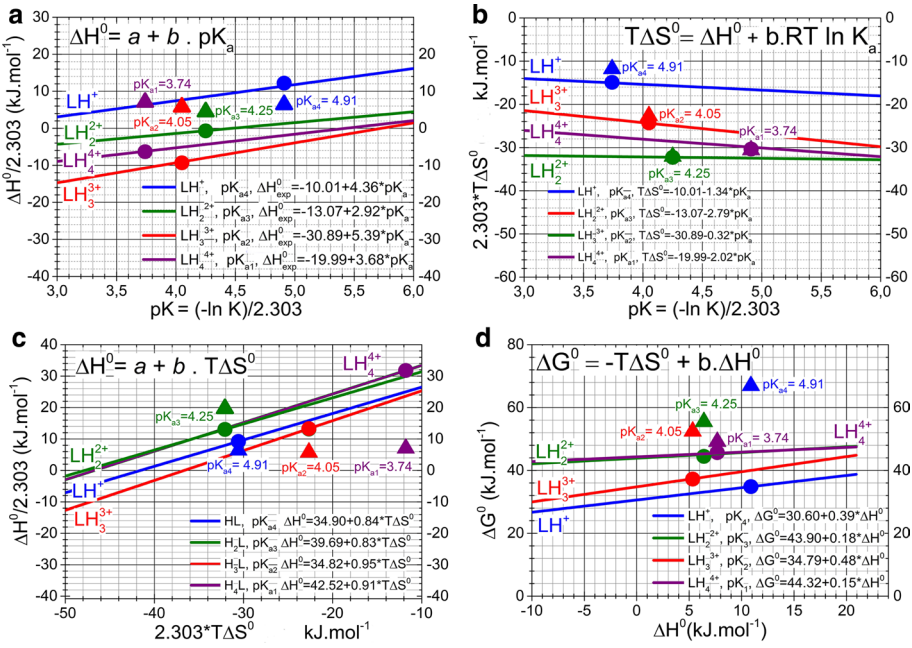

Fig. 12 Graphical presentation of QSARs *extrathermodynamics* concerning dissociation of four cations for the prediction of the actual thermodynamics of Nilotinib (triangles) in comparison with their experimental values (full circles): *graph* ***a*** $\Delta H° = a + b \cdot pK_a$, *graph* ***b*** $T\Delta S° = \Delta H° + b \cdot RT\ \ln\ K_a$, *graph* ***c*** $\Delta H° = \Delta G° + b \cdot T\ \Delta S°$, and *graph* ***d*** $\Delta G° = -T\Delta S° + b \cdot \Delta H°$. Each figure contains four straight lines for LH^+, LH_2^{2+}, LH_3^{3+}, and LH_4^{4+} for the prediction of the actual thermodynamics of Nilotinib (full circles)

Therefore, these graphs could also serve as a convenient criterion for the reliability of experimentally determined estimates of enthalpy, entropy and Gibbs energy.

In the equation $\Delta H^\circ = \Delta G^\circ + b{\cdot}T\Delta S$ (Fig. 12b), the estimated slope b is usually said to be the "extent" to which the entropy compensates the enthalpy. We have remarked that a strong correlation between ΔH° and ΔS° is not, by itself, a proof of true ΔH° versus ΔS° compensation arising from *chemical causality*, but that instead it could be an artefact due to the transmission of experimental errors. In fact, ΔS° was essentially obtained by calculating it from the thermodynamic dissociation constant, and that of ΔH° was determined by van´t Hoff plots. As a consequence, any error on ΔH° will affect the error on ΔS°. Hydrogen bond rearrangement, then, could underlie both ΔH° and ΔS° in drug–proton interactions and an interrelationship between ΔH° and ΔS° seems plausible, indeed likely. This suggests that the apparent *enthalpy–entropy compensation*, which was observed experimentally, "…arose from an intrinsic property of the hydrogen bond…" namely "…that any tightening of the intermolecular bonds (*the enthalpic factor*) was compensated by a loss of degrees of freedom (*the entropic factor*), or vice versa". Generally speaking, a stronger intermolecular interaction or bonding (related to the enthalpy) would lead to a greater reduction of configurational freedom and hence greater order of the system (related to the entropy). This might be the cause of the enthalpy–entropy compensation.

On Fig. 12 the graphs yield some common conclusions which may be commonly elucidated with agreement of Ref. [8]:

(1) When pK_a is positive, the standard Gibbs energy change ΔG° for the dissociation reaction is also positive and may be decomposed using the ΔH° versus pK_a dependence and the $T\Delta S^\circ$ versus pK_a dependence. The ΔH° versus pK_a plot shows that the ΔH° value is sensitive to changes in pK_a because of electrostatic effects. With increasing the BrØnsted basicity of the drug (*i.e.*, increasing pK_a of an actual drug), the ΔH° term increases and the $T\Delta S^\circ$ term decreases (Fig. 12a, b).

(2) The positive value of ΔH° indicates that the dissociation process is endothermic and is accompanied by an absorption of heat. As ΔH° becomes more negative (stronger bonding), ΔS° tends to decrease due to the tightening up of the system (Fig. 12c). When ΔH° becomes less negative (weaker bonding), ΔS° tends to increase as the system becomes increasingly disordered. The hydrogen bond rearrangement, then, could underlie both ΔH° and ΔS° in drug–proton interactions and an interrelationship between ΔH° and ΔS° seems plausible, indeed likely. The hydrogen bond as central to a drug–proton interaction also is mechanistically appealing. In water, the hydrogen bonds form a network of continuous chains that are dynamically changing (in a sort of steady state). Because of the dipole created by displacement of the electron from the hydrogen proton, these chains form a sequence of mono- and dipoles that are sensitive to the electrostatic potential of the drug and receptor molecules and provide a mechanism for transmitting information at a distance from drug to receptor.

(3) When ΔH° is negative, then the value $T\Delta S^\circ$ is the dominant factor, which determines whether ΔG° is positive (Fig. 12d).

4) The entropy contribution is mostly unfavorable ($\Delta S^\circ < 0$) in these reactions (Fig. 12c). Ions in an aqueous solution tend to orient the surrounding water molecules, which orders the solution and decreases the entropy. The contribution of an ion to the entropy is the partial molar entropy which is often negative, especially for small or highly charged ions. The ionization of an acid involves reversible formation of two ions so that the entropy

decreases ($\Delta S^\circ < 0$). There are now four cations on the reversible ionization of the same acid and the anion has a charge, so the entropy again only decreases.

5 Discussion

The REACTLAB and SQUAD84 regression programs analyzed the pH–absorbance matrix of 1×10^{-4} mol·L^{-1} Nilotinib hydrochloride and provided quantified estimates of four dissociation constants with two different numerical approaches. Both programs showed successful conclusions of goodness-of-fit tests with four dissociation constants being better than that for three dissociation constants.

The results of protonation/dissociation constants refinement could include information concerning the goodness of fit of the residual-sum-of-squares function *RSS*, the parameter estimates calculated, the standard deviations of parameters and the correlation coefficients between them, the residuals map, and the concentrations of all the species in the model for all data points. The model selection [71] was the process of deciding whether to accept the results. Usually all of the above factors should be taken into account, since no one of them on its own is a reliable indicator of the success or failure of the calculation.

The ESAB program minimizing residuals $e_i = V_{\mathrm{exp},i} - V_{\mathrm{calc},i}$, reached residual values of about 0.1 or 0.2 μL, indicating an excellent curve fitting of the calculated titration curves through experimental points. It can be stated that the reliability of dissociation constants of Nilotinib hydrochloride has been proven, although the *group parameters* L_0, H_T were ill-conditioned in the nonlinear regression model. The good curve fitting showed sufficient reliability of the estimates of all four dissociation constants of Nilotinib hydrochloride at 25 °C and 37 °C.

The inconsistency of the experimentally found pK_{ai} estimates and their theoretically predicted values could be due to the complicated structure of the resonance of the heterocyclic nucleus, and consequently to the different electron distributions, which might further lead to different predicted pK_{ai} values according to the structural formula of the molecule. In such cases, the prognostic programs MARVIN, PALLAS and ACD/Percepta might fail, so the dissociation constants needed to be definitely determined experimentally. Given that the pK_{ai} estimates of both potentiometric and spectrophotometric methods were similar and, most importantly, plausible in terms of achieved fitness in the data regression, it can be concluded that the experimental results obtained are reliable and show the real dissociation of the substance.

6 Conclusion

(1) Spectrophotometric and potentiometric pH titration allowed measurement of up to four closely similar dissociation constants of Nilotinib hydrochloride (Scheme 1). Nilotinib hydrochloride chromophores exhibited small changes of absorbance in UV/VIS spectra when adjusting the pH of the solution, and therefore estimates of dissociation constants were subject to greater uncertainty than for the potentiometric determination. For this reason, a more reliable estimation of the dissociation constants appear ti be obtained potentiometrically.

(2) Nilotinib hydrochloride denoted as L was capable of protonation in pure water to produce four soluble species LH^+, LH_2^{2+}, LH_3^{3+}, and LH_4^{4+}. The graph of the molar

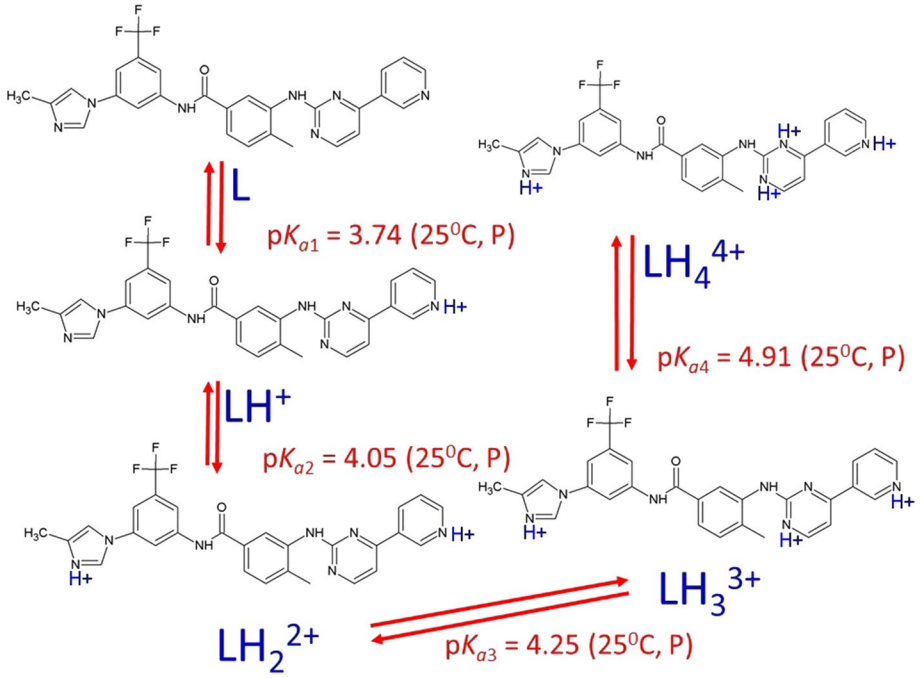

Scheme 1 Protonation scheme of Nilotinib hydrochloride

absorption coefficients of differently protonated species in relation to wavelength indicated that the spectrum of ε_L, ε_{LH}, ε_{LH2}, ε_{LH3}, and ε_{LH4} were for two pairs of correlated species and values in each pair were almost the same.

(3) It has been demonstrated that in the range of pH 2 to 7, four dissociation constants can be reliably estimated from the spectrum when the concentration of the sparingly soluble Nilotinib hydrochloride was 1.0×10^{-4} mol·L^{-3}. Although the adjusted pH affected the absorbance changes in the chromophore less, four thermodynamic dissociation constants were reliably determined, with SQUAD84 and REACTLAB reaching similar values for both programs, $pK^T_{a1}=3.60\pm0.04$, $pK^T_{a2}=4.42\pm0.07$, $pK^T_{a3}=4.71\pm0.04$, and $pK^T_{a4}=4.84\pm0.03$ at 25 °C and $pK^T_{a1}=3.61\pm0.11$, $pK^T_{a2}=4.29\pm0.18$, $pK^T_{a3}=4.49\pm0.02$, and $pK^T_{a4}=5.05\pm0.03$ at 37 °C.

4) The four thermodynamic dissociation constants of Nilotinib hydrochloride were determined by regression analysis of potentiometric titration curves at a potentiometric concentration of 3×10^{-4} mol· L^{-1} with ESAB, $pK^T_{a1}=3.74\pm0.01$, $pK^T_{a2}=4.05\pm0.01$, $pK^T_{a3}=4.25\pm0.01$, and $pK^T_{a4}=4.91\pm0.20$ at 25 °C and $pK^T_{a1}=3.63\pm0.03$, $pK^T_{a2}=3.96\pm0.03$, $pK^T_{a3}=4.18\pm0.03$, and $pK^T_{a4}=4.81\pm0.05$ at 37 °C (Fig. 11).

(5) Prediction of the dissociation constants of Nilotinib hydrochloride was performed by the programs MARVIN, PALLAS and ACD/Percepta to determine the protonation sites. When comparing three predictive and two experimental techniques, prognostic programs sometimes differed in their pK_a estimates.

(6) Thermodynamic parameters $\Delta H°$ and $\Delta G°$ were calculated from the temperature change of dissociation constants according to the van't Hoff equation. Positive enthalpy values $\Delta H°$ at 25 °C show that the dissociation process is endothermic and is accompanied by absorption of heat. As entropy values of the dissociation processes $\Delta S°$ at

25 °C and 37 °C were negative, the dissociation process is reversible. The *compensation effect* should only mean that there is a linear relationship between the enthalpy and entropy changes of a series of a dissociation of acids in aqueous solutions. For often observed large compensation effects, especially those involving solution or variously protonated anions, redistribution of the energy-distinguishable subspecies is most likely the physical origin. These findings seem to point to the idea that the enthalpy–entropy compensation found arises from an intrinsic property of the hydrogen bond, which is the main force determining the association of the participants (water, drug, binding site) in the drug–receptor binding equilibrium. This idea simply reflects the more basic fact that any tightening of the intermolecular bonds (the enthalpic factor) is compensated by a loss of degrees of freedom (the entropic factor), or vice versa. The ionization of a neutral acid involves formation of two ions so the entropy decreases. There are now three ions on the second ionization of the same acid and the anion has a charge, so the entropy again can only decrease. The compensation analysis could also be a useful tool for investigating pharmaceutical and chemical processes of relevance to QSAR of drugs.

References

1. Gora-Tybor, J., Robak, T.: Targeted drugs in chronic myeloid leukemia. Curr. Med. Chem. **15**(29), 3036–3051 (2008)
2. IUPAC Compendium of Chemical Technology—the Gold Book, Version 2.3.3, 2014-02-254. IUPAC Secretariat, Research Triangle Park, NC
3. Pandey, M.M., Jaipal, A., Kumar, A., Malik, R., Charde, S.Y.: Determination of p*K*(a) of Felodipine using UV-visible spectroscopy. Spectrochim. Acta A **115**, 887–890 (2013)
4. Milletti, F., Storchi, L., Sforna, G., Cruciani, G.: New and original p*K*a prediction method using grid molecular interaction fields. J. Chem. Inf. Model. **47**, 2172–2181 (2007)
5. Manallack, D.T.: The p*K*(a) distribution of drugs: application to drug discovery. Perspect. Med. Chem. **1**, 25–38 (2007)
6. Settimo, L., Bellman, K., Knegtel, R.A.: Comparison of the accuracy of experimental and predicted p*K*a values of basic and acidic compounds. Pharm. Res. **31**, 1082–1095 (2014)
7. Tam, K.Y., Takacs-Novak, K.: Multiwavelength spectrophotometric determination of acid dissociation constants: a validation study. Anal. Chim. Acta **434**, 157–167 (2001)
8. Meloun, M., Ferenčíková, Z.: Enthalpy–entropy compensation for some drugs dissociation in aqueous solutions. Fluid Phase Equil. **328**, 31–41 (2012)
9. Sillén, L.G., Warnqvist, B.: Equilibrium constants and model testing from spectrophotometric data using Letagrop. Acta Chem. Scand. **22**(9), 3001–3034 (1968)
10. Sillén, L.G., Warnqvist, B.: High-speed computers as a supplement to graphical methods. 7. Model selection and rejection with Letagrop. Elimination of species with negative or insignificant equilibrium constants. Ark Kemi **31**(4), 341–352 (1969)
11. Sillén, L.G., Warnqvist, B.: High-speed computers as a supplement to graphical gethods. 6. A strategy for 2-level Letagrop adjustment of common and group parameters Some features that avoid divergence. Ark Kemi **31**(4), 315–339 (1969)
12. Sillén, L.G., Warnqvist, B.: High-speed computers as a supplement to graphical methods. 10. Application of Letagrop to spectrophotometric data, for testing models and adjusting equilibrium constants. Ark Kemi **31**(4), 377–390 (1969)
13. De Stefano, C., Princi, P., Rigano, C., Sammartano, S.: Computer analysis of equilibrium data in solution ESAB2 M: an improved version of the ESAB program. Ann. Chim. (Rome) **77**(7–8), 643–675 (1987)
14. Rigano, C., Grasso, M., Sammartano, S.: Computer-analysis of equilibrium data in solution—a compact least-squares computer-program for acid–base titrations. Ann. Chim. (Rome) **74**(7–8), 532–537 (1984)

15. Alderighi, L., Gans, P., Ienco, A., Peters, D., Sabatini, A., Vacca, A.: Hyperquad simulation and speciation (HySS): a utility program for the investigation of equilibria involving soluble and partially soluble species. Coord. Chem. Rev. **184**, 311–318 (1999)
16. Gans, P., Sabatini, A., Vacca, A.: Investigation of equilibria in solution. Determination of equilibrium constants with the HYPERQUAD suite of programs. Talanta **43**(10), 1739–1753 (1996)
17. Gans, P., Sabatini, A., Vacca, A.: Hyperquad computer-program suite. Abstr. Pap. Am. Chem. Soc. **219**, U763–U763 (2000)
18. Gans, P., Sabatini, A., Vacca, A.: Simultaneous calculation of equilibrium constants and standard formation enthalpies from calorimetric data for systems with multiple equilibria in solution. J. Solution Chem. **37**(4), 467–476 (2008)
19. Allen, R.I., Box, K.J., Comer, J.E.A., Peake, C., Tam, K.Y.: Multiwavelength spectrophotometric determination of acid dissociation constants of ionizable drugs. J. Pharm. Biomed. Anal. **17**(4–5), 699–712 (1998)
20. Hartley, F.R., Burgess, C., Alcock, R.M.: Solution Equilibria. Ellis Horwood, Chichester (1980)
21. Leggett, D.J., McBryde, W.A.E.: General computer program for the computation of stability constants from absorbance data. Anal. Chem. **47**(7), 1065–1070 (1975)
22. Kankare, Jouko J.: Computation of equilibrium constants for multicomponent systems from spectrophotometric data. Anal. Chem. **42**(12), 1322–1326 (1970)
23. Ribeiro, A.R., Schmidt, T.C.: Determination of acid dissociation constants (p*K*(a)) of cephalosporin antibiotics: computational and experimental approaches. Chemosphere **169**, 524–533 (2017)
24. ACD/Labs p*K*a Predictor 3.0. In: Inc., A.C.D. (ed.). Toronto, Canada (2007)
25. Balogh, G.T., Gyarmati, B., Nagy, B., Molnar, L., Keseru, G.M.: Comparative evaluation of in silico p*K*(a) prediction tools on the gold standard dataset. QSAR Comb. Sci. **28**(10), 1148–1155 (2009)
26. Balogh, G.T., Tarcsay, A., Keseru, G.M.: Comparative evaluation of p*K*(a) prediction tools on a drug discovery dataset. J. Pharm. Biomed. Anal. **67–68**, 63–70 (2012)
27. Evagelou, V., Tsantili-Kakoulidou, A., Koupparis, M.: Determination of the dissociation constants of the cephalosporins Cefepime and Cefpirome using UV spectrometry and pH potentiometry. J. Pharm. Biomed. Anal. **31**(6), 1119–1128 (2003)
28. Liao, C.Z., Nicklaus, M.C.: Comparison of nine programs predicting p*K*(a) values of pharmaceutical substances. J. Chem. Inf. Model. **49**(12), 2801–2812 (2009)
29. Roda, G., Dallanoce, C., Grazioso, G., Liberti, V., De Amici, M.: Determination of acid dissociation constants of compounds active at neuronal nicotinic acetylcholine receptors by means of electrophoretic and potentiometric techniques. Anal. Sci. **26**(1), 51–54 (2010)
30. Bezencon, J., Wittwer, M.B., Cutting, B., Smiesko, M., Wagner, B., Kansy, M., Ernst, B.: p*K*(a) determination by H-1 NMR spectroscopy—an old methodology revisited. J. Pharm. Biomed. Anal. **93**, 147–155 (2014)
31. Hansen, N.T., Kouskoumvekaki, I., Jorgensen, F.S., Brunak, S., Jonsdottir, S.O.: Prediction of pH-dependent aqueous solubility of drug like molecules. J. Chem. Inf. Model. **46**(6), 2601–2609 (2006)
32. Manchester, J., Walkup, G., Rivin, O., You, Z.P.: Evaluation of p*K*(a) estimation methods on 211 drug like compounds. J. Chem. Inf. Model. **50**(4), 565–571 (2010)
33. ten Brink, T., Exner, T.E.: p*K*(a) based protonation states and microspecies for protein–ligand docking. J. Comput. Aid. Mol. Des. **24**(11), 935–942 (2010)
34. Meloun, M., Syrový, T., Bordovská, S., Vrána, A.: Reliability and uncertainty in the estimation of p*K*(a) by least squares nonlinear regression analysis of multiwavelength spectrophotometric pH titration data. Anal. Bioanal. Chem. **387**(3), 941–955 (2007)
35. Meloun, M., Bordovská, S., Vrána, A.: The thermodynamic dissociation constants of the anticancer drugs camptothecine, 7-ethyl-10-hydroxycamptothecine, 10-hydroxycamptothecine and 7-ethylcamptothecine by the least-squares nonlinear regression of multiwavelength spectrophotometric pH-titration data. Anal. Chim. Acta **584**(2), 419–432 (2007)
36. Meloun, M., Bordovská, S., Syrový, T., Vrána, A.: Tutorial on a chemical model building by least-squares non-linear regression of multiwavelength spectrophotometric pH-titration data. Anal. Chim. Acta **580**(1), 107–121 (2006)
37. Meloun, M., Pilařová, L., Pekárek, T., Javůrek, M.: Overlapping p*K*(a) of the multiprotic hemostyptic eltrombopag using UV-Vis multiwavelength spectroscopy and potentiometry. J. Solution Chem. **46**(11), 2014–2037 (2017)
38. Meloun, M., Čápová, A., Pilařová, L., Pekárek, T.: Multiwavelength UV-metric and pH-metric determination of the multiple dissociation constants of the Lesinurad. J. Pharm. Biomed. Anal. **158**, 236–246 (2018)
39. Maeder, M., King, P.: Analysis of Chemical Processes, Determination of the Reaction Mechanism and Fitting of Equilibrium and/or Rate Constants. https://www.intechopen.com/books/c (2012)

40. Meloun, M., Čapek, J., Mikšík, P., Brereton, R.G.: Critical comparison of methods predicting the number of components in spectroscopic data. Anal. Chim. Acta **423**(1), 51–68 (2000)
41. ORIGIN.: OriginLab Corporation, One Roundhouse Plaza, Suite 303, Northampton, MA 01060, USA (2019)
42. Krotz-Vogel, W., Hoppe, H.C.: The PALLAS parallel programming environment. Lect. Notes Comput. Sci. **1332**, 257–266 (1997)
43. Meloun, M., Pilařová, L., Čápová, A., Pekárek, T.: The overlapping thermodynamic dissociation constants of the antidepressant Vortioxetine using UV–VIS multiwavelength pH-titration data. J. Solution Chem. **47**(5), 806–826 (2018)
44. Meloun, M., Nečasová, V., Javůrek, M., Pekárek, T.: The dissociation constants of the cytostatic Bosutinib by nonlinear least-squares regression of multiwavelength spectrophotometric and potentiometric pH-titration data. J. Pharm. Biomed. Anal. **120**, 158–167 (2016)
45. Meloun, M., Pilařová, L., Bureš, F., Pekárek, T.: Multiple dissociation constants of the Interpirdine hydrochloride using regression of multiwavelength spectrophotometric pH-titration data. J. Mol. Liq. **261**, 480–491 (2018)
46. Rodante, F., Fantauzzi, F.: Thermodynamic analysis of the ionization of ortho and para toluic acids—influence of the medium on the hyperconjugative and steric effects. Thermochim. Acta **109**(2), 353–365 (1987)
47. Hu, J.H., Zhuang, P., Lin, R.S., Xie, Y.S.: Ionization thermodynamics of methylbenzoic acids in water–DMF mixtures. Thermochim. Acta **262**, 227–231 (1995)
48. Nan, Y.Q., Yu, Q.S., Lin, R.S.: Thermodynamics of ionization of *o*-fluoro and *o*-chloro benzoic acids in water–ethanol mixtures at 298.15 K. Thermochim. Acta **317**(2), 201–203 (1998)
49. Hu, X.G., Li, S.Q., Lin, R.S., Zong, H.X.: Enthalpic and entropic contributions to substituent effects on the ionization of meta- and para-nitrobenzoic acids in EtOH–H_2O mixtures at 298.15 K. Thermochim. Acta **319**(1–2), 43–45 (1998)
50. Hu, X.G., Lin, R.S., Zong, H.X.: Ionization thermodynamics of methylbenzoic acids in EtOH–H_2O mixtures. Thermochim. Acta **326**(1–2), 1–5 (1999)
51. Gruber, C., Buss, V.: Quantum mechanically calculated properties for the development of quantitative structure-activity-relationships (QSARs)—p*K*a values of phenols and aromatic and aliphatic carboxylic-acids. Chemosphere **19**(10–11), 1595–1609 (1989)
52. Trapani, G., Carotti, A., Franco, M., Latrofa, A., Genchi, G., Liso, G.: Structure affinity relationships of some alkoxycarbonyl-2H-pyrimido[2,1-B]benzothiazol-2-ones or alkoxycarbonyl-4H-pyrimido[2,1-B]benzothiazol-4-ones benzodiazepine receptor ligands. Eur. J. Med. Chem. **28**(1), 13–21 (1993)
53. Shusterman, A.J.: Predicting mutagenicity—use a technique thats been useful in predicting efficacy. ChemTech **21**(10), 624–627 (1991)
54. Debnath, A.K., Shusterman, A.J., Decompadre, R.L.L., Hansch, C.: The Importance of the hydrophobic interaction in the mutagenicity of organic-compounds. Mutat. Res. **305**(1), 63–72 (1994)
55. Aguerre, R.J., Suarez, C., Viollaz, P.E.: Enthalpy–entropy compensation in sorption phenomena—application to the prediction of the effect of temperature on food isotherms. J. Food Sci. **51**(6), 1547–1549 (1986)
56. Gabas, A.L., Menegalli, F.C., Telis-Romero, J.: Water sorption enthalpy–entropy compensation based on isotherms of plum skin and pulp. J. Food Sci. **65**(4), 680–684 (2000)
57. Gabas, A.L., Telis-Romero, J., Menegalli, F.C.: Thermodynamic models for water sorption by grape skin and pulp. Dry. Technol. **17**(4–5), 961–974 (1999)
58. Labuza, T.P.: Enthalpy–entropy compensation in food reactions. Food Technol. **34**(2), 67–77 (1980)
59. Sugihara, G., Hisatomi, M.: Enthalpy–entropy compensation phenomenon observed for different surfactants in aqueous solution. J. Colloid Interf. Sci. **219**(1), 31–36 (1999)
60. Liu, L., Guo, Q.X.: Isokinetic relationship, isoequilibrium relationship, and enthalpy–entropy compensation. Chem. Rev. **101**(3), 673–695 (2001)
61. Schmid, R., Miah, A.M., Sapunov, V.N.: A new table of the thermodynamic quantities of ionic hydration: values and some applications (enthalpy–entropy compensation and Born radii). Phys. Chem. Chem. Phys. **2**(1), 97–102 (2000)
62. Goodman, M.F.: Hydrogen bonding revisited: geometric selection as a principal determinant of DNA replication fidelity. Proc. Natl. Acad. Sci. USA **94**(20), 10493–10495 (1997)
63. Lumry, R., Rajender, S.: Enthalpy–entropy compensation phenomena in water solutions of proteins and small molecules: a ubiquitous property of water. Biopolymers **9**(10), 1125–1227 (1970)
64. Dunitz, J.D.: Win some, lose some—enthalpy–entropy compensation in weak intermolecular interactions. Chem. Biol. **2**(11), 709–712 (1995)

65. Meloun, M., Havel, J., Högfeldt, E.: Computation of Solution Equilibria: A Guide to Methods in Potentiometry, Extraction, and Spectrophotometry. Ellis Horwood Series in Analytical Chemistry. Ellis Horwood Chichester, England (1988)
66. Meloun, M., Ferenčíková, Z., Javůrek, M.: Reliability of dissociation constants and resolution capability of SQUAD(84) and SPECFIT/32 in the regression of multiwavelength spectrophotometric pH-titration data. Spectrochim. Acta A **86**, 305–314 (2012)
67. Meloun, M., Militký, J., Forina, M.: Chemometrics for Analytical Chemistry: PC-aided Regression and Related Methods, vol. 2. Ellis Horwood, Chichester (1994)
68. Leggett, D.J., Kelly, S.L., Shiue, L.R., Wu, Y.T., Chang, D., Kadish, K.M.: A computational approach to the spectrophotometric determination of stability constants—II. Application to metalloporphyrin-axial ligand interactions in non-aqueous solvents. Talanta **30**(8), 579–586 (1983)
69. Meloun, M., Militký, J., Forina, M.: Chemometrics for Analytical Chemistry, : PC-Aided Statistical Data Analysis, Chemometrics for Analytical Chemistry, vol. 1. Ellis Horwood, Chichester (1992)
70. Meloun, M., Militký, J.: Statistical Data Analysis: A Practical Guide, Complete with 1250 Exercises and Answer Key on CD, 1st edn. Woodhead Publishing Limited, 80 High Street Sawstone Cambridge, CB22 3HJ, UK, New Delhi, Oxford, Philadelphia (2011)
71. Meloun, M., Bartoš, M., Högfeldt, E.: Multiparametric curve fitting. 13. Reliability of formation-constants determined by analysis of potentiometric titration data. Talanta **35**(12), 981–991 (1988)